A Reconfigurable Antenna based on a Non-radiative Dielectric Waveguide with a Liquid Crystal Dielectric

Thesis submitted in partial fulfillment
of the requirements for the degree of

Master of Science

in

Electrical Engineering
track Telecommunications

by

Wilfred Lourens Boelhouwer
born in Amsterdam, The Netherlands

Committee members:

prof.dr. Alexander Yarovoy	Supervisor TU Delft
dr. ing. Peter Knott	Supervisor Fraunhofer FHR
dr. ir. Bert-Jan Kooij	TU Delft
dr. Daniele Cavallo	TU Delft

Date of MSc defense: February 12, 2016

TU Delft Delft University of Technology

Fraunhofer FHR

Delft University of Technology
Department of
Microelectronics

The undersigned hereby certify that they have read and recommend to the Faculty of Electrical Engineering, Mathematics and Computer Science for acceptance a thesis entitled **"A Reconfigurable Antenna based on a Non-radiative Dielectric Waveguide with a Liquid Crystal Dielectric"** by **Wilfred Lourens Boelhouwer** in partial fulfillment of the requirements for the degree of **Master of Science**.

Dated: February 12, 2016

Chairman:

prof.dr. Alexander Yarovoy

Committee Members:

dr. ing. Peter Knott

dr. ir. Bert-Jan Kooij

dr. Daniele Cavallo

Abstract

A frequency-pattern reconfigurable antenna based on a foreshortened non-radiative dielectric (NRD) waveguide structure with a tunable liquid crystal dielectric is proposed. The antenna operates within the full range of the unlicensed 60G-band.

The antenna is fed by a stripped semi-rigid coaxial feed that is inserted directly into the liquid crystal dielectric. The feed is positioned either asymmetrically near the antenna's end or symmetrically in the antenna's center resulting in a single or double conical radiation pattern respectively.

Full-wave numerical solver simulations have been carried out with the help of CST Microwave Studio to evaluate the characteristics of both the symmetrically and asymmetrically fed antenna. The liquid crystals have been modelled as an isotropic homogeneous dielectric that can assume different values of effective dielectric permittivity.

For both structures it can be concluded that the main beam of the radiation pattern can be steered across an angle between 20° and 50° for various combinations of frequency and dielectric constant for a minimum antenna gain of 15dB. Furthermore an 800MHz instantaneous (-3dB) bandwidth is realistic.

The asymmetric and symmetric structure show a vastly different input reflection (S_{11}) response. The symmetric structure is matched across almost the full 7GHz bandwidth of the unlicensed 60G-band, regardless of the assumed value of dielectric permittivity. The asymmetric structure on the other is only matched for a select bandwidth interval (approximately 1GHz) that shifts for each assumed dielectric permittivity value.

Foreword

This thesis is the result of an extended period of work and research which I started in March 2012 under the supervision of dr. ing. Peter Knott in the Fraunhofer Institute for High Frequency Physics (FHR) in Wachtberg, Germany and dr. Massimiliano Simeoni as supervisor from my home university, the Delft University of Technology. In 2013 I returned to the Netherlands, continuing my efforts under the supervision of prof. dr. Alexander Yarovoy and partial supervision of dr. Diego Caratelli.

Acknowledgements

I would hereby like to take the opportunity to thank all the people that have been involved in the process of writing this thesis.

First and foremost I extend my gratitude towards my final responsible supervisor prof. dr. Alexander Yarovoy. I will remember him as the person who during my academic career has made the strongest impact on my level of knowledge with regards to my knowledge of antennas, microwaves and electromagnetism, both in his role of teacher and supervisor. Furthermore, I have come to know him as a persion who demonstrates patience and the willingness to listen. I will remember the time he took to discuss not only matters that were relevant to this thesis but also other questions relating to electomagnetism in general.

I would further like to thank dr. ing. Peter Knott. I have experienced Peter to be both a patient instructor as well as a good-tempered and approachable man who provided the right boundary conditions for a very pleasant stay in Germany at the FHR institute. Moreover I am particularly grateful for the opportunity he has given to fabricate a static leaky-wave antenna in the mechnical workshop and for bringing me into contact with the Technical University of Darmstadt.

Furthermore my thanks go out to dr. Massimiliano Simeoni, my lecturer in antenna systems and former supervisor who presented me the opportunity to perform my research in the FHR institute by bringing me into contact with Peter Knott. Also, my thanks go out to dr. Diego Caratelli who was willing to take over this role in a later stage.

Thanks go out to dr. ing. Christian Damm, dr. ing. Matthias Maasch and M.Sc. María Roig Parras for allowing me to perform experiments at the Technical University of Darmstadt (Germany) on two occasions. Similarly, I would like to say my thanks to Christian Schuster, a local student and now my friend, who so kindly offered me a place to stay during the experiments.

Particular thanks go out to my friend Nelleke Koffeman whose divine intervention and support helped me through the last stages of writing this thesis by being a beacon of guidance, support and good conscience.

Another special thank you goes out to my friend Merel Brouns for designing a formidable front cover of this thesis. I am strongly impressed by the way in which she has been able to create a majestical artist impression of the studied antenna.

Finally, I would like to extend my gratitude to my parents and my sister, Kees, Marijke and Emma. The patience and understanding they have shown during the hard times has been legendary.

Contents

List of Figures

1 Introduction

1.1 Background & motivation

Traditionally, wireless radio systems were designed for a single-mission purpose. Accordingly, the antennas that have supported such systems possessed static characteristics, i.e. a fixed frequency of operation, radiation pattern and polarization [3].

Starting in the 80s reconfigurable antennas have been gaining significant interest [4]. Such antennas possess the capability to change the mentioned characteristics on-mission. Consequently, this technological development has enabled a trend towards multi-functional wireless systems [5].

An example of a reconfigurable antena is discussed in [1] and shown in Figure 1.1 where the operating frequency of a printed dipole antenna can be switched through optical switches placed on the dipole arms. Illuminating the switch by a laser causes the switch to conduct, resulting in an increased length of the dipole. As a result the resonance frequency is shifted[1].

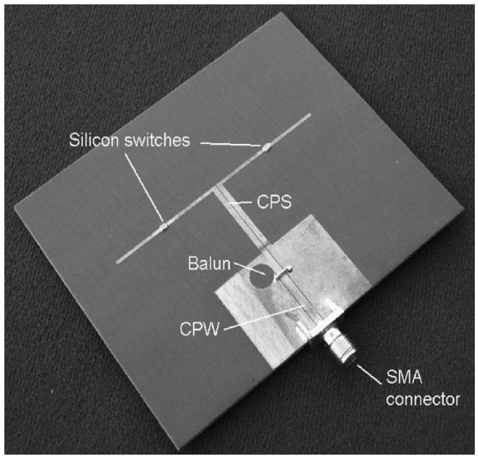

Figure 1.1: Reconfigurable printed dipole antenna with optical switches [1]

Reconfigurable antennas are far from an academical curiosity. Reconfigurability has found applications in the support of multiple wiress standards [3], beam focussing [6] without the usage of phased arrays and dynamic spectrum re-allocation [5]. Indeed a single reconfigurable antenna can replace several ones with a single function.

[1]The resonance frequency can be switched between 2.26GHz and 3.15GHz

The state-of-the-art in reconfigurable antennas can be described either according to the reconfigured parameter (as mentioned above) or the reconfiguration method. Available methods are switchable (electrical and optical) elements (e.g. RF MEMS, pin-diodes, varactors), physical structure alternation (e.g. bending) and material changes (e.g. liquid crystals (LC)) as is described in [4] and shown in Figure 1.2.

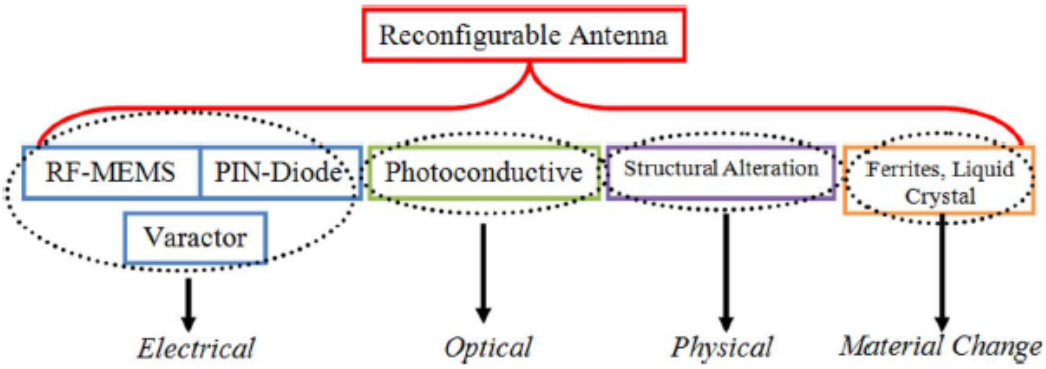

Figure 1.2: Methods of reconfiguration

Electrical & optical reconfiguration Electrical and optical switching elements lend themselves well for frequency reconfiguration [3]. They can be attributed an open/short circuited state (MEMS) or an on/off-state (PIN diodes, photoconductive switches) [4]. In this manner multi-band antenna's can be realized by effectively changing the antenna's electrical size and corresponding resonance frequency.

One example is a dual-band dipole-on-silicon antenna where the effective dipole arm length is changed with the aid of MEMS (similar to the example in Figure 1.1). This allows for frequency reconfiguration between 4.86GHz and 8.98GHz (85%) [7].

Another example is the 3x3-array of microstrip patches (connected by MEMS) in [8] where a more drastic reconfiguration from the L- to X-band is possible by opening/-closing all switches[2].

The main advantage of the electrical switching mechanisms is their ease of integration in an antenna structure whereas their main disadvantage is the additional complexity introduced by the biasing circuitry. Optical switches on the other hand are less popular since they require a relatively complex activation mechanism[3] [4].

Physical reconfiguration Physically reconfigurable antennas derive their functionality from structural deformation. They are mentioned here for sake of completeness with respect to the categorization made in [4]. Their obvious advantage lies in the fact that these antennas do not require biasing circuitry. One interesting example is a leaky-wave antenna based on a mechanically tunable impedance surface that is excited

[2]The source [8] mentions reconfiguration from $1-2$GHz to $8-12.5$GHz but exact resonance frequencies are not given.

[3]A more detailed comparison of switching techniques is beyond the scope of this thesis but can be found in [4].

by an external waveguide. The antenna features an impressive 45° tunable range at 2.5GHz [9].

Material change Antennas that can be reconfigured by tuning of their material properties. These materials include ferrites, ferro-electric and (nematic) liquid crystals. Ferrites feature a tunable magnetic permeability μ_r whereas ferro-electrics and liquid crystals feature a tunable electric permittivity ϵ_r [4]. The relative advantage of liquid crystals compared to ferrites and ferro-electric materials (such as Barium-Strontium-Titate) is their improving efficiency for higher frequencies (i.e. decreasing loss tangent) [10].

Antennas featuring a liquid crystal dielectric have been actively researched in the past decade. Since the antenna proposed in this thesis is based on liquid crystals as well it is in order to discuss some examples of prior research.

Two examples of frequency reconfigurable antennas operating in a relatively low frequency range are discussed in [11] and [12]. They are microstrip patch antennas featuring a liquid crystal layer between patch and ground plane. The resonance frequency can be steered from 2.16GHz to 2.08GHz (3.7%) and from 5.75GHz to 5.3GHz (7.8%) respectively[4]. Another example is shown in [13] where reconfiguration of 4.74GHz to 4.6GHz (3.9%) is achieved for a different liquid crystal mixture. Note that the given resonance frequencies shift from higher to lower frequencies, corresponding to a change from unbiased to biased state.

Pattern reconfigurability has also been demonstrated using liquid crystals. One approach is a reconfigurable reflectarray of patch antennas in which the cavity between patch and groundplane is filled with liquids crystals while the patches are externally excited by a waveguide. Examples of this approach can be found in [14] (35 GHz) and [10] (77GHz) where 40° and 50° of scanning has been realized[5].

Yet another example of pattern reconfigurability is a so-called tunable composite right/left-handed leaky-wave antenna handed based on a rectangular waveguide with a liquid crystal dielectric as introduced in [15]. Here, 20° of tuning around broadside has been achieved around 7.6GHz.

1.2 Objectives and approach

Reconfigurable antennas are an active field of research as has been established in the previous section. Various methods of reconfiguration have already been actively researched (Figure 1.2). The antenna proposed in this thesis attempts to make a contribution to this.

More specifically, this thesis has the following twofold objective:

[4] Radiation effiencies are rather poor (35% and 25%) due to the high loss tangent.

[5] The ostensibly large scanning angles should be weighed carefully because of the main beam degradation. Moreover, only one-dimensional instead of two-dimensional scanning is achieved.

1. Investigation of the possibilities for a single antenna to cover the full unlicensed 60GHz-band by frequency tunability. An instantaneous bandwidth of up to 1GHz is ambitioned.
2. Achievement of pattern reconfigurability (beam scanning) without employing a phased array for the same frequency band.

In order to achieve this objective the following approach has been used:

1. An antenna topology based on a leaky waveguide is selected. Simultaneously, a choice is made for liquid crystals to be employed as a tunable dielectric. The particular combination of leaky-wave antenna topology and a liquid crystal tunable dielectric make a strong candidate for achieving the joint objective of frequency and pattern reconfiguration as described above (Sections 1.3 and 2.5).
2. Two specific prototypes with a particular feed position/type and specific geometric dimensions are derived based on basic design considerations (Chapters 3 and 4).
3. The relevant antenna properties (gain, input reflection, bandwidth) are computed by performing full wave numerical simulations over the frequency range and the tunable values of the liquid crystals (Chapter 5). This is done with the help of the CST Microwave Studio solver package.

Finally, a conclusion is drawn by evaluating the proposed antenna. This is done through mutual comparison of both feed approaches by analyzing the simulation data.

1.3 Proposed antenna

In this thesis a pattern-frequency reconfigurable antenna based on non-radiative dielectric (NRD) guide (Figure 1.3b) antenna topology and tunable liquid crystals operating at the unlicensed European 60GHz-band (Figure 1.3a) has been studied.

More specifically, the NRD waveguide is transformed into a leaky-wave antenna by decreasing the top gap to an electrically small size. In this fashion energy "leaks" away from the top, thereby realizing a radiating structure, i.e. an antenna. In turn, the dielectric itself consists of the liquid crystal. A voltage applied to the plates steers the crystals in such a way that a tunable dielectric is realized.

Two specific structures are derived having an asymmetric and symmetric coaxial feed that injects energy into the dielectric crystals, thereby exciting the waveguide.

The asymmetric structure relies on the constructive interference of the direct wave and the wave reflected from the dielectric-air interface close to the feed. The symmetric structure simply features two bi-directional waves. The liquid itself is contained by the conducting plates and an electromagnetically invisible foam container. A qualitative schematic of the setup (of the asymmetric feeding situation) is shown in Figure 1.4[6].

[6]The ratios of the real structure are not represented accurately in this figure. The structure itself is very elongated.

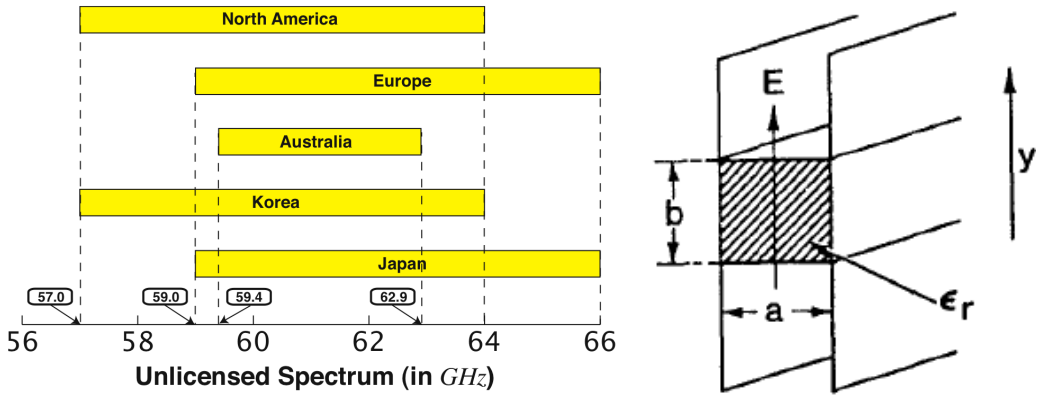

(a) Unlicensed 60-GHz spectrum (b) Foreshortened NRD

Figure 1.3: Choice of antenna type and frequency band

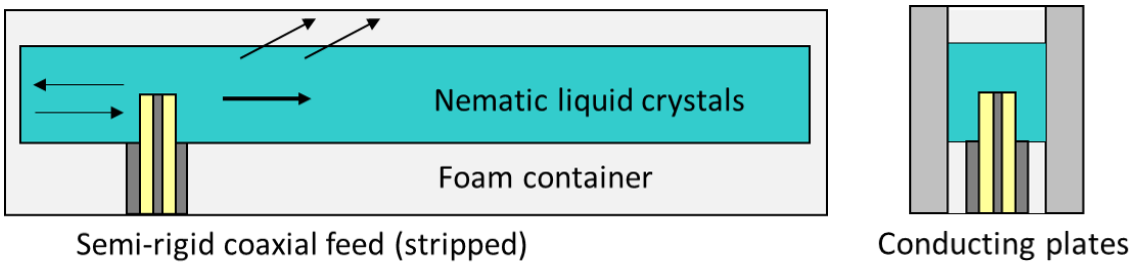

(a) Longitudinal view (b) Cross section

Figure 1.4: Qualitative schematic overview (asymmetric feeding)

The resulting radiation pattern features a single or double conical beam around the longitudinal axis and can be tuned by either tuning the dielectric permittivity ϵ_r of the liquid crystals or by changing the operational frequency f_0.

The radiation pattern of the asymmetric antenna is shown Figure 1.5. Figure 1.5a gives a qualitative impression of the conical radiation pattern for the center tuning state where $(\epsilon_r, f_0) = (2.8, 62.5\text{GHz})$ whereas Figure 1.5b shows the radiation pattern behavior for several tuning states.

The motivation for the design choices (antenna type, type of dielectric, frequency band) that have been made is given in chapter 2 and can be summarized as follows:

- A leaky-wave antenna is a suitable candidate for frequency-pattern reconfiguration by a tunable dielectric since the antenna's radiation pattern is inherently dependent on both the operating frequency and the dielectric constant.
- Liquid crystals display acceptable tunability and low-loss behavior at very high frequencies.
- The 60GHz- unlicensed band is promising for future (short range) high datarate applications [16].

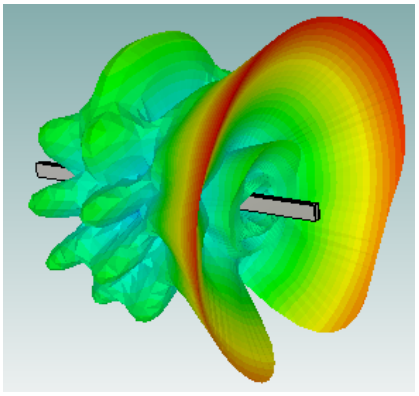

(a) 3-dimensional radiation pattern w.r.t. structure orientation (asymmetric feeding, single beam)

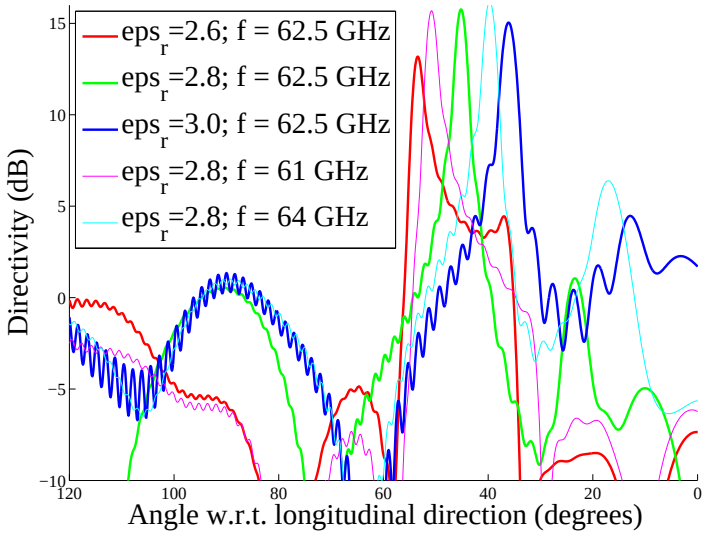

(b) Several tuning states (principal plane)

Figure 1.5: Pattern-frequency tunable radiation pattern

1.4 Thesis structure

The current introductory chapter describes the background of the work, a brief motivation and a summary of the most important results.

In chapter 2 the particular choice for NRD waveguide technology and liquid crystal material is motivated.

In chapter 3 the proposed structure is specified: structure dimensions, liquid crystal type and feeding is selected based on realistic design considerations.

In chapter 4 waveguide parameters are derived based on internal waveguide analysis.

In chapter 5 the relevant antenna characteristics (Gain, S_{11}) as a function of tuning state are computed for both antenna structures with the help of a full-wave solver.

Finally, in chapter 6 the work is concluded by answering the question to which extent the added functionality provided by dielectrical tuning is of sufficient interest for further exploration.

Leaky-wave antennas & liquid crystals

2

This chapter explains the particular choice for an NRD (leaky) waveguide structure with LC dielectric. First it is explained in section 2.1 why leaky-wave antennas are generally good canditates for dielectric reconfiguration. Second an overview of leaky-wave antenna types and innovation is given in section 2.2. Then several tunable materials are discussed in section 2.4 and finally the selection of topology and tunable material (NRD waveguide, liquid crystals) is made in section 2.5.

2.1 Why leaky-wave antennas?

A leaky-wave antenna is a good candidate for frequency-dielectric reconfiguration: its radiation pattern depends on the excited leaky wavenumber k_z which in turn is a function of frequency (f) and material such as dielectric constant ϵ_r.

2.1.1 What is a LWA?

A leaky-wave antenna is a waveguide that has been modified in such a way that energy is allowed to leave its structure. In other words, a guiding structure is turned into a radiating element. Additionally, since this radiation occurs in a gradual fashion as the wave travels one can think of the structure to be leaky, hence the name: leaky-wave antenna. Alternatively, the IEEE provides an acceptible definition as well: "An antenna that couples power in small increments per unit length either continuously or discretely, from a traveling wave structure to freespace" [17].

An illustrative example of such a modification is a typical rectangular waveguide that has been opened up from the side wall. Although energy is still largely confined to the guide, the internal field weakens as the wave travels and energy escapes through the opening (fig. 2.1).

To be precise, the structure above belongs to the class of one-dimensional uniform leaky-wave antennas. Due to its simplicity it serves well to illustrate the principal leaky-wave antenna features.

2.1.2 Features

The leaky-wave antenna's main benefit is that it features a tunable radation pattern: a frequency-scannable main beam. This is a direct consequence of a leaky-wave antenna's

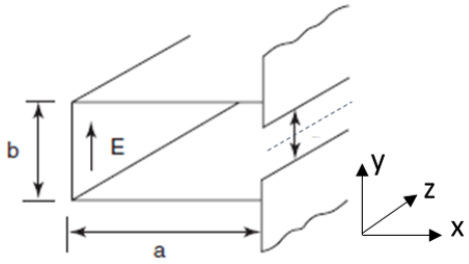

Figure 2.1: Rectangular waveguide made leaky through sidewall slit

phase variation across its aperture. To illustrate this let one assume the aperture field of the structure in Figure 2.1 to be described by the magnetic current line:

$$K(z) = K_0 \exp(-jk_z z) \quad (0 < z < \infty) \tag{2.1}$$

$$k_z = \beta_z - j\alpha_z \quad (\beta_z < \beta_0) \tag{2.2}$$

The aperture field described by (2.1) is an exponentially decaying waveform with a superluminal phase velocity (2.2). The shape of such a waveform is shown in Figure 2.2a assuming a particular value for the phase constant β_z and two different values for the attenuation α_z.

The radiation pattern resulting from the aperture distribution can be described best by a fan-beam that radiates in the upper halfspace. This pattern is elegantly described by (2.3)[1] [18] and plotted in fig. 2.2b for its principal plane[2]. For simplicity, the line current is assumed to be infinitely long.

$$|E_\phi(r,\theta)| = |K_0 \cdot \psi(r) \cdot \frac{\sin\theta}{\cos\theta - \frac{k_z}{k_0}} \cdot (1 - e^{-j(k_z - k_0\cos\theta)l})| \tag{2.3}$$

It is important to note that the leaky-wavenumber k_z determines the important features of the radiation pattern: β determines the angle whereas α determines the sidelobe level and the amount of (un)radiated energy. This can be directly observed from Figure 2.2b.

In turn the leaky-wavenumber k_z itself is determined by both the operating frequency as well as the geometry of the structure. This is an intricate relationship that is described by a so-called dispersion relation.

For any fixed structure (and corresponding dispersion relation) the phase constant beta is positively related to the frequency. Hence, an increase of frequency corresponds to an increase of β. In turn an increase of β implies an antenna beam that is steered away from broadside to endfire as could already be observed in Figure 2.2b. In fact, for small values of α the main beam direction is succinctly approximated by

$$\theta_m = \arccos(\frac{\beta}{\beta_0}). \tag{2.4}$$

[1] The pattern description results from assuming the presence of an infinite groundplane.
[2] An additional radiation pattern pair with a different β_z is plotted for comparison.

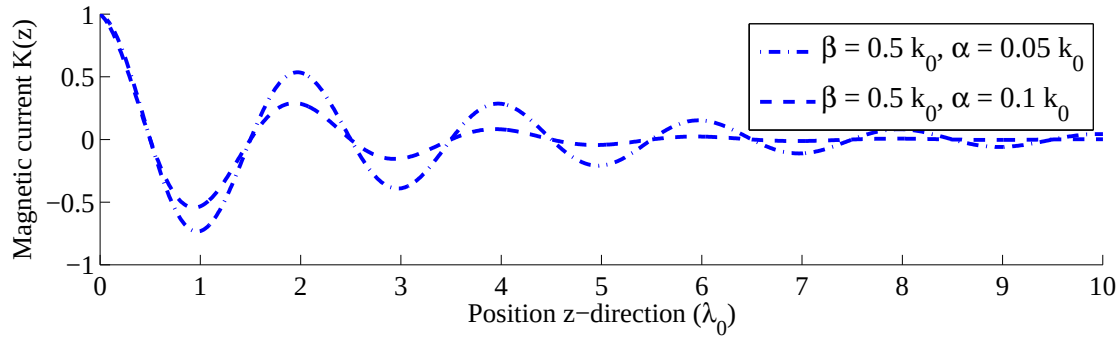

(a) Normalized magnetic current vs. position ($\Re\{K(z)\}$ of Eq. (2.1))

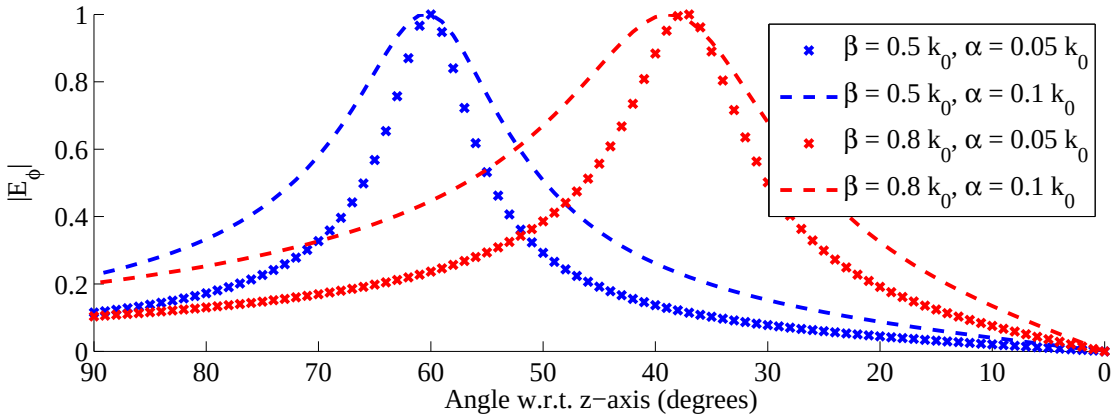

(b) Normalized radiation pattern

Figure 2.2: Magnetic line source representing aperture in Figure 2.1

Concluding, a leaky-wave antenna features a radiation pattern that is frequency dependent. By changing the operating frequency or dielectric constant one can thus tune the antenna.

2.2 Leaky-wave antennas: classification & innovation

2.2.1 Classification

Leaky-wave antennas can be classified in certain ways that provide insight in their fundamental properties. Classication by the shape of the cross-section (uniform or periodic) and the direction of wave propagation (1D or 2D) are particularly useful.

Uniform leaky-wave antennas are characterized by a cross-section with a longitudinally constant shape. The structure in figs. 2.1 and 2.3a is the most direct example of this. A similar structure where the broader side is loaded with a stub is shown in fig. 2.3b [17]. Leaky-wave antennas based on open structures are possible as well such

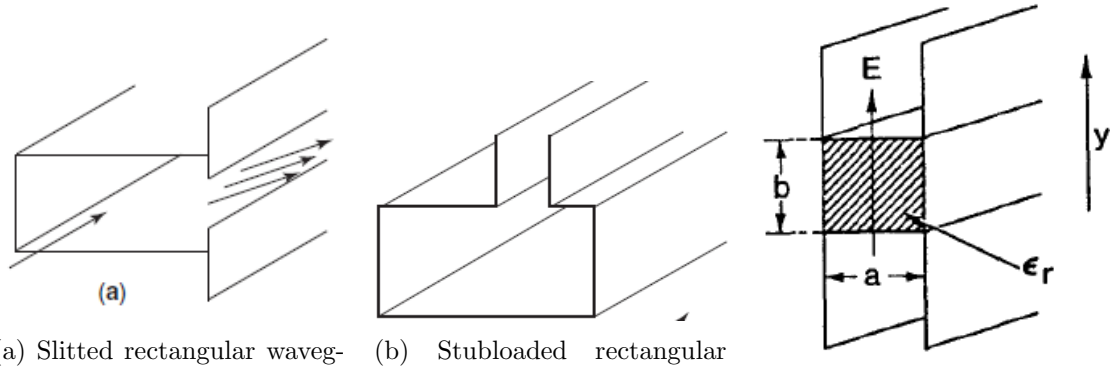

(a) Slitted rectangular waveguide

(b) Stubloaded rectangular waveguide

(c) Foreshortened NRD guide

Figure 2.3: Leaky-wave antennas with uniform cross-section

as the foreshortened non-radiative dielectric (NRD) guide [3] shown in fig. 2.3c [17, 19].

The characteristic feature of a homogeneous structure is an aperture that is described by a single fast wave leaky-wavenumber k_z. This allows for radiation into the forward quadrant only. Moreover, broadside as well as endfire radiation is problematic.

Broadside radiation corresponds to a β_z of zero, or equivalently a standing wave, implying operation at the antennas cutoff frequency. As for endfire radiation, this state is approached as $\beta_z \to \beta_0$, which generally coincides with an attenuation that approaches zero, resulting in the necessity of electrically very long structures.

In direct contrast there exists a group of LWAs that are characterized by their periodicity. They are derived from guiding structures that are inherently non-leaky. Leakage is introduced through the (periodical) modulation of the original structure. In this manner, a fundamentally slow wave is expanded into an infinite series of so-called space-harmonics, a single of which is actually a fast wave accounting for leaky-wave radiation. The advantage of this class of periodic LWAs is that they can scan through both the forward and the backward quadrant, with the exception of broadside.

Examples include a grounded dielectric image guide, modulated with periodic grooves or metal strips (fig. 2.4a) [17], a slotted parallel plate structure (fig. 2.4b) [20] or a microstripline structure with periodically spaced resonators or stubs (fig. 2.4c) [17].

Through careful design, the fast space harmonic that causes the radiation can have a positive as well as negative phase constant β_z. This allows for radiation into the upper hemisphere, however with the same restriction on broadside radiation as with the uniform structures.

Another possibility for classification is made possible through the distinction between 1D and 2D wave propagation. Most LWAs such as the ones shown feature a wave propagating in a single direction with a corresponding (longitudinal) (leaky) wavenumber. A leaky-wave may however also be radially propagating through a structure, away from a centrally located source point.

[3] Open structure tend to be preferable for higher frequencies due to increasing ohmic losses

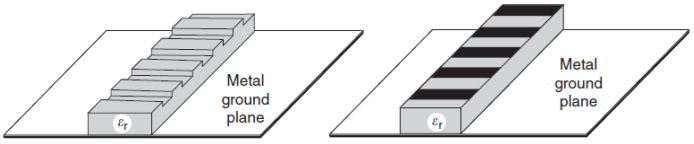

(a) Dielectric image guide

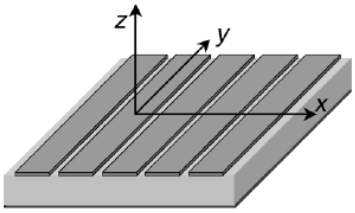

(b) Slotted parallel plate guide

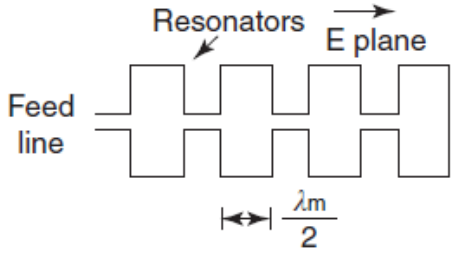

(c) Microstrip with resonating patches

Figure 2.4: Periodically modulated leaky-wave antennas

Possible configurations include a substrate-superstrate configuration or a partially reflective surface [18, 21] as can be seen in figs. 2.5a and 2.5b. Through design these structures allow for a broadside pencil beam that evolves into a conical pattern for other frequencies.

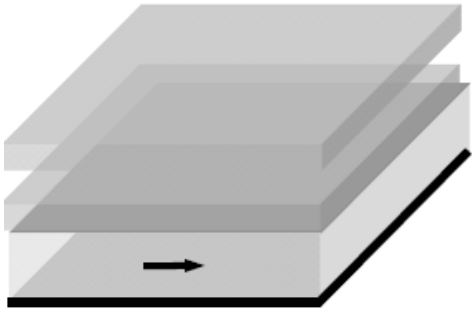

(a) Substrate-superstrate configuration

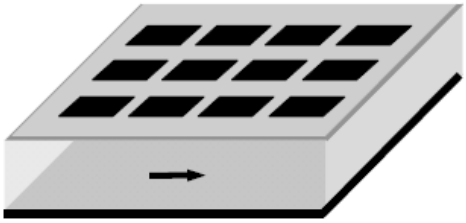

(b) Metallic patches

Figure 2.5: Leaky-wave antennas with 2-dimensional wave propagation

The properties of the several leaky-wave antenna classes are succinctly summarized in table 2.1

Class	Pattern shape	Scan range	Broadside
Uniform (1D)	Cone-pencil	90 deg.	no
Periodic (1D)	Cone-pencil	180 deg.	no
2D	Pencil-cone	90 deg.	yes

Table 2.1: Leaky-wave antenna classes and principal properties

2.3 State-of-the-art leaky-wave antennas and further innovation

In section section 2.1.2 the principal leaky-wave antenna features have been described. In spite of its generally desirable frequency tunability there also exist drawbacks such as an inability to provide broadside radiation. This section describes some recent leaky-wave antenna innovations. This provides insight in the current paths of development that leaky-wave antennas are going through.

Metamaterials The employment of metamaterials as leakywave structures resembles a revoluation in leaky-wave antenna design. They provide an elegant solution to the classical limitation on broadside radiation [2, 22].

Metamaterials are composite materials that display unnatural properties on the macroscopic scale [2]. These properties are generally realized by means of a periodic disturbance of an otherwise homogenous material. The periodicity is necessarily much smaller than the wavelength of the wave supported by the structure [22, 23].

This has resulted in a gamechanging leaky-wave antennastructure that is called the Circularly Right/Left-handed LWA. It features a beam that is scannable through the forward and backward quadrant, including broadside if the structure is balanced (i.e. $-k_0 < \beta_{lw} < k_0$). An equivalent circuit of a small stretch of fundamental period length is shown in fig. 2.6.

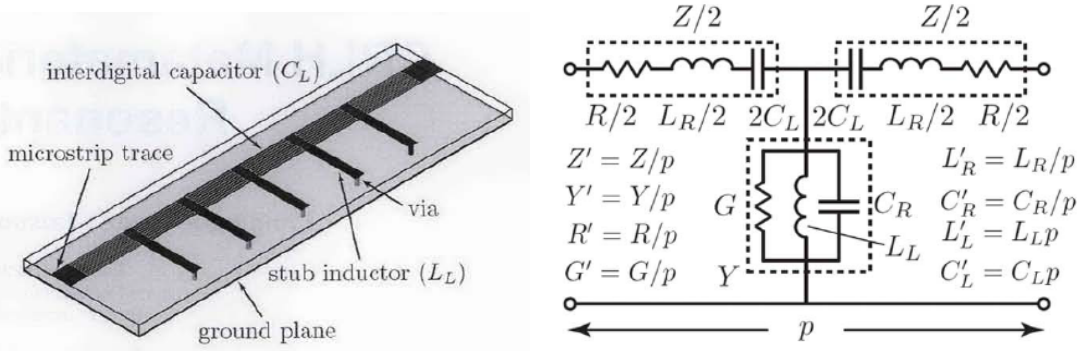

(a) Structure impression

(b) Transmissionline circuit model

Figure 2.6: Circularly right/left-handed leaky-wave antenna based on microstripline [2]

The operation of this type of leaky-wave antennacan be summarized as follows:

1. Forward radiation: caused by periodic stubs determining the series inductance and shunt capacitance.
2. Backward radiation: caused by periodic interdigital capacitors and vias determining series capacitance and shunt inductance respectively (in addition to some amount of radiation).
3. Through proper dimensioning an effective phase constant of zero resulting in broadside radiation can be achieved.

Impedance transformation The CRLH leaky-wave antennabased on metamaterial structures allows for broadside radiation through the fundamental guided mode. Later, it was discovered that this could also be achieved for a true perodic leaky-wave antennaradiating through a fast space harmonic [22, 24].

This has been achieved by ensuring the fundamental cell of the structure to be matched to the line at broadside frequency. This in turn is achieved through a relatively conventional approach: the cell is enhanced by adding a delay line and a quarter-wave transformer. This can be observed in fig. 2.7 where the indicated distances d_1 and d_2 correspond to the mentioned additions to the structure.

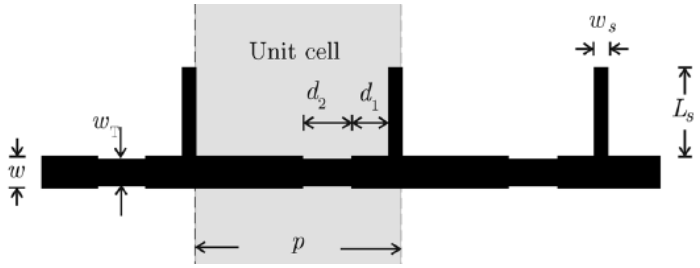

Figure 2.7: Impedance matched microstrip leaky-wave antenna with radiating stubs

Substrate integrated waveguide The two structures under discussion are based on microstrip technology. This is not surprising as an antenna's usefulness strongly depends on its integrability in a full microwave system. However, to this end there exists another promising technology: Substrate-Integrated Waveguide (SIW). It is considered a promising candidate for higher frequencies due to better loss performance compared to conventional microstrip technology [22, 25, 26].

Moreover, based on this waveguiding platform, leaky-wave antennas can be derived as well.

SIW technology is a guiding structure in which a substrate is sandwiched between two conducting planes, connected through (cylindrical) metal vias that act as side walls. Such a structure can be viewed as a dielectrically loaded (rectangular) waveguide from the electromagnetical perspective. Indeed, the fundamenal mode of operation is the fast TE10-mode.

Leaky-wave antennas can be derived from the SIW technology. One way is to allow leakage through the sidewall by increasing the distance between succesive vias [25]. Another way is through the incission of slots on the top wall [22, 27]. The advantage of the latter solution is its ability to radiate well at endfire. However it should be noted that the main purpose of using SIW technology is its inherently better low-loss performance.

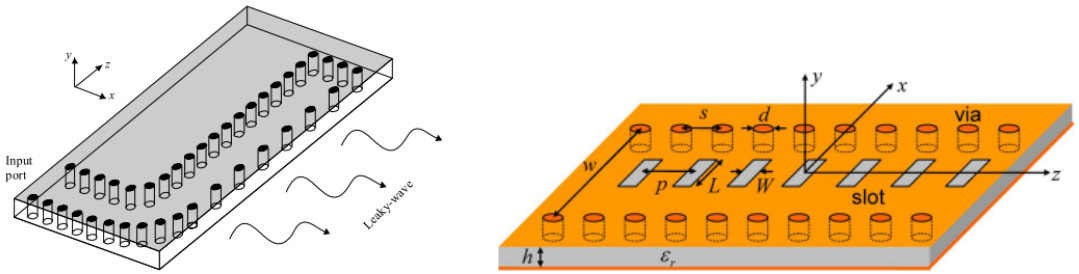

(a) Side leakge through gaps in vias (b) Top leakge through transverse slots

Figure 2.8: Leaky-wave antennas based on Substrate-integrated Waveguide

2.4 Tunable materials

2.4.1 Tunable material comparison

A tunable material is required that allows for changing the wavelength inside a structure. The specific need for continuous tuning of permittivity ϵ_r by means of an electrical field essentially limits the possible materials to either nematic liquid crystals or Barium-Strontium-Titanate (BST).

BST is a solid crystal structure in which ions can be moved through (strong) external fields [28]. Liquid crystals have a crystallic structure as well, however feature a semi-liquid state in a certain temperature range. A certain sense of order is present, yet the molecules can be easily steered through external field. In addition, the (oblong) molecules show anisotropic behavior.

The anistropy of liquid crystals can be exploited for microwave applications [4]. LCs sandwiched between a parallel plate structure can be assigned a default orientation by applying a groove like structure to the plates (the untuned state). Then, the molecules can be continuously tuned by applying a static voltage as is shown in fig. 2.9.

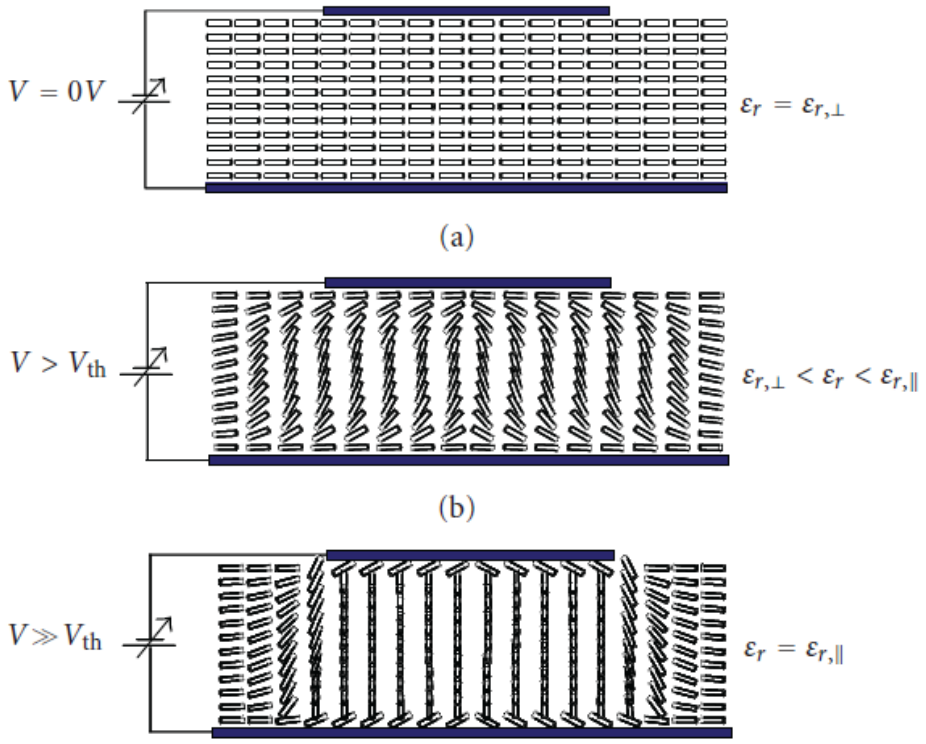

Figure 2.9: Orientation of liquid crystals through an external electric field

If one supposes the presence of an (additional) RF-field propagating throughout the structure in fig. 2.9 then a (macroscopic) dielectric constant ϵ_r is experienced that is dependent of the angle between the electric (RF-) field and the orientation of the molecules. In other words, a tunable dielectric is achieved with its tuning range defined as $\epsilon_{r,\perp} < \epsilon_{r,eff} < \epsilon_{r,\parallel}$.

It is desirable to introduce quality metrics for a tunable dielectric such as has been

[4]Note that this has already done for optical applications, the LCD display being a famous example

Type	Tunable range	Tunability τ	Req. field strength	Quality factor η
LC	$2.4 < \epsilon_r < 3.4$	$< 24\%$	750V/cm	10-100 GHz:30
BST	$1000 < \epsilon_r < 5000$	$< 90\%$	20kV/cm	1GHz:50-100, 10GHz:25

Table 2.2: Comparison LC and BST dielectrics

done in [28]. First one defines tunability τ to quantify the atainable tuning range (2.5). Second, one defines a quality factor η as the ratio of tunability τ and loss tangent $\tan\delta$ (2.6).

$$\tau = \frac{\epsilon_{r,\parallel} - \epsilon_{r,\perp}}{\epsilon_{r,\parallel}} \tag{2.5}$$

$$\eta = \frac{\tau}{\tan\delta} \tag{2.6}$$

With the aid of above metrics LC and BST can be put in comparison. Consequently, information has been aggregated from several sources and is displayed in table 2.2 [10, 28, 29]. Generalizing one can say that LCs offer a limited tunability τ up to extremely high frequencies. BST features an inverse behavior. The very high dielectric constants as well as the limited frequency behavior of BST make LCs the tuning material of choice for the desired (unlicensed 60GHz) frequency band.

2.4.2 Selection of liquid crystal mixture

In order to proceed, it is necessary to obtain realistic values for the dielectric constants by using nematic liquid crystals.

Unfortunately data is relatively difficult to find since LCs are still mostly used in optical applications. Information is scattered across academical publications such as [30], [29] and [10]. Moreover, there exists some discrepancy in listed dielectric constants[5].

An LC-mixture has been selected based on its frequency of appearance in the literature as well as its predicted tunability: BL006 (produced by MERCK). In [30] measurements of the dielectric constants have been performed from 3 to 40 GHz and it turns out ϵ_r displays a flat behavior. In this work, this behavior is extrapolated into the 60 GHz range and hence the values listed in the source are assumed to be correct. These measurement results are displayed in fig. 2.10 and the derived BL006-values in table 2.3.

[5]For example: the K15 LC-mixture possesses a relative permittivity of $2.55 \rightarrow 2.85$ and $2.3 \rightarrow 2.57$ according to [10] and [29] respectively.

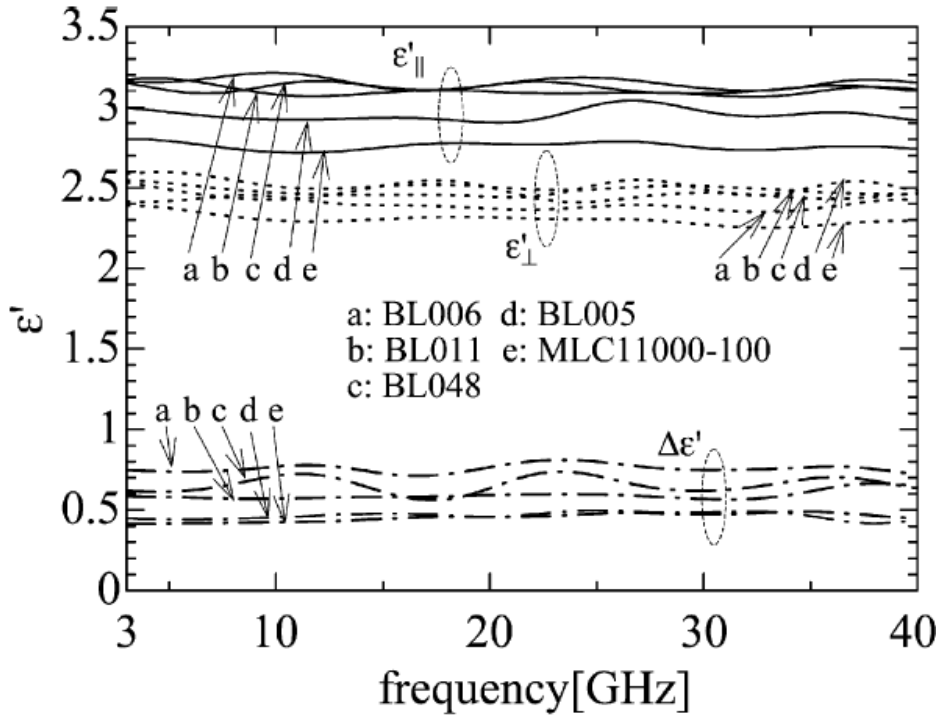

(a) Tunability vs. frequency

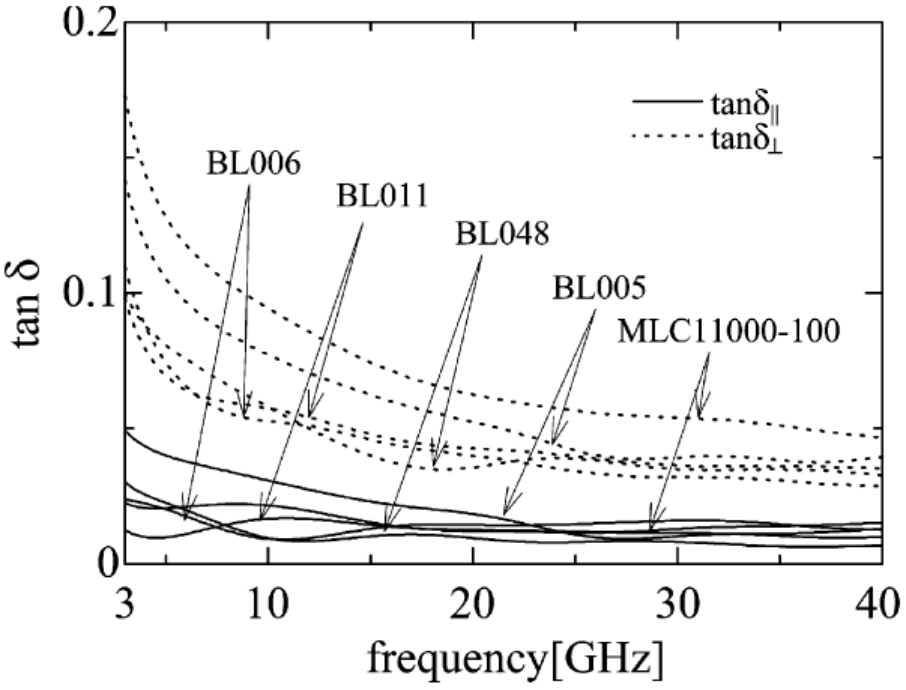

(b) Loss tangent

Figure 2.10: Frequency behavior for several LC-mixtures

Name	$\epsilon_{\parallel}$	$\epsilon_{\perp}$	$\tan\delta_{\parallel}$	$\tan\delta_{\perp}$
BL006	3.03	2.62	0.01	0.22

Table 2.3: LC characteristics

2.5 Selection: NRD Waveguide & Liquid Crystals

leaky-wave antenna The NRD waveguide topology has been selected. The first reason is its parallel plate structure. This is a necessity since electrical tuning requires the application of a static voltage across the dielectric without creating a short-circuit. The second reason is that its one-dimensional uniform structure is relative simple both from the analytical as fabrication point of view.

tunable dielectric Liquid crystals are the preferred type of tunable dielectric compared to BST as has been explained in the previous section.

In chapter 3 an actual antenna structure will be derived from the chosen topology.

Antenna prototype

3

3.1 Foreshortened NRD with liquid crystal dielectric

A foreshorted non-radiative dielectric (NRD) guide with a nematic liquid crystal dielectric is proposed. They feature relatively low dielectrical constants and good loss behavior at higher frequencies. In addition, they can be tuned by means of a relatively low external voltage.

The NRD-guide is first introduced by Sanchez and Oliner in [19] in which it is described how shortening one end transforms an NRD-guide into a leaky-wave antenna. Normally the structure consists of a static dielectric rod squeezed between two conducting plates.

In the proposed structure, the dielectric consists of nematic liquid crystals, kept in place by a foam-like container. The wave is launched by means of a coaxial probe. Furthermore, a static field across the plates allows for tuning the relative permittivity. Finally, the frequency band of operation is proposed to be the 60GHz-band.

Two specific antenna structures will be presented based on the design choices that have been made. They share a common antenna topology, dielectric and LC container. They differ in feed position and transverse shape.

1. symmetric: centrally located feed → split beam
2. asymmetric: feed located on one end → direct and reflected wave

The antenna is realized by means of a cavity cut into a foam-like sheet, pressed firmly in between a pair of rectangular conducting plates. The coaxial feed is positioned either in the center or at one of the long ends as indicated in Figure 3.1 and inserted through the foam from below.

The proposed alternatives differ in feeding position, resulting in a symmetric or asymmetric structure. The symmetric structure is characterized by a wave travelling in opposite directions. The asymmetric structure features a direct and a reflected wave that are constructively added for a certain frequency.

Aspect	Design choice	Remark
Topology	Foreshorted NRD-guide	Leakage by plate shortening
Dielectric	Nematic liquid crystals	Dielectric constants between 2.5 → 3.5
Feed	Coaxial probe	Semi-rigid
Frequency	60G Unlicensed band	$f_c = 62.5$GHz

Table 3.1: Design choice overview

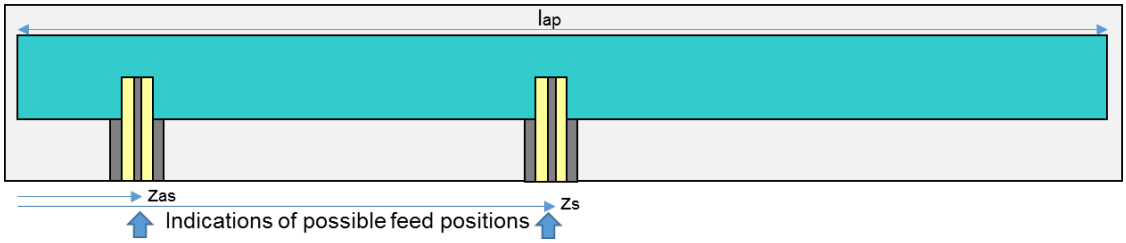

(a) Longitudinal view

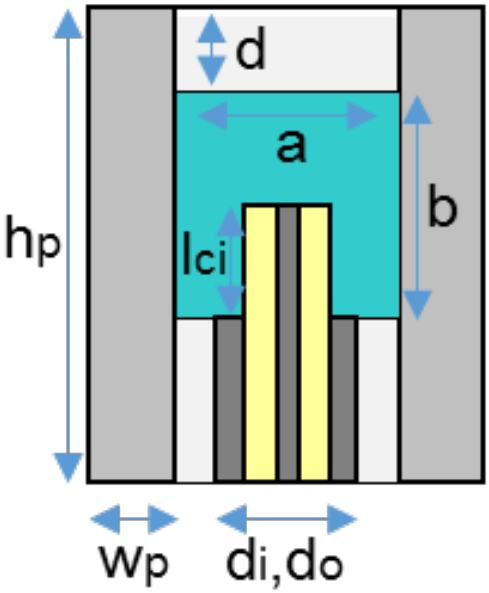

(b) Transversal view

Figure 3.1: Possible coaxial probe positions (symmetric and asymmetric structure) and parameter symbols

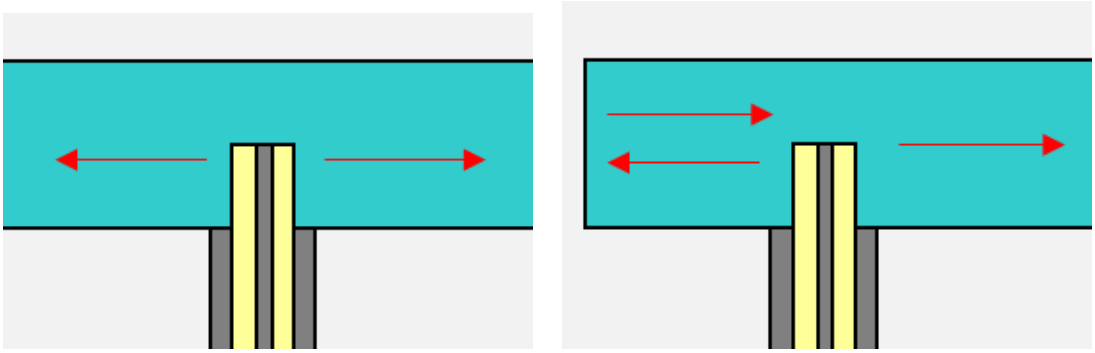

(a) Center: lateral excitation

(b) Side: constructive interference

Figure 3.2: Close-up of feed positions and relevant dimensions

3.2 Parameters to be determined

The proposed structures require a determination of parameters. Parameters are either established as a result from an optimization procedure, an assumption or a selection from a list (e.g. in case of standardized components such as coaxial feeds (appendix D.1)). The chosen values are shown in Table 3.2. Elaboration on establishing the shown values is done in the next chapter.

Parameter	Symbol	Value	Follows from
Dielectric	ϵ_r	$2.6 \rightarrow 3.0$	section 2.4.2
Dielectric width, height	a,b	2.0mm, 2.04mm	chapter 4
Gap	d	0.5mm	chapter 4
Aperture length	l_{ap}	180 mm	chapter 4
Plate width, height	w_p, h_p	1 mm, 8 mm	assumption
Coaxial inner/out diameter	d_i, d_o	0.29 mm, 1.14 mm	standardized
Coaxial dielectric	$\epsilon_{r,c}$	2.1	component
Coaxial insertion length	$l_{c,i}$	0.9 mm	chapter 4

Table 3.2: Parameter overview

3.3 Choice of feed & frequency

Feed Two types of feeding have been investigated that result in the excitation of a leaky-wave:

1. rectangular waveguide (mounted in front of nrd)
2. coaxial feed (injected from bottom)

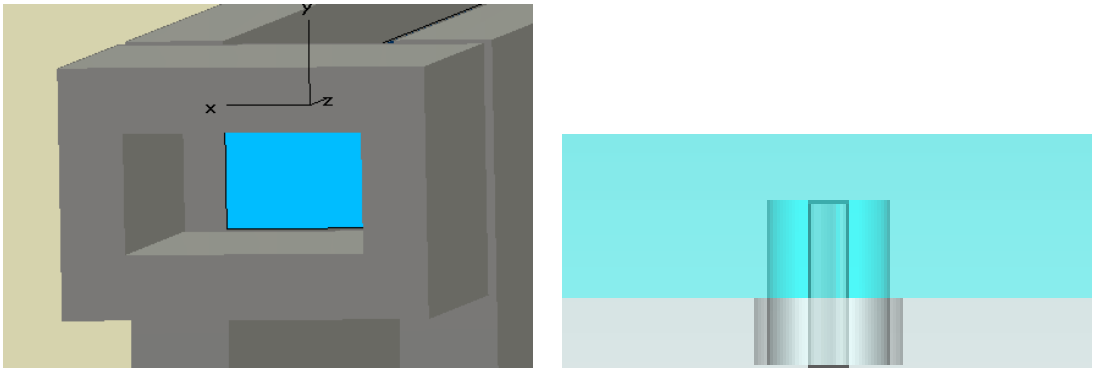

(a) Rectangular guide (positioned in front) (b) Coaxial probe (inserted into dielectric)

Figure 3.3: Schematic overview of feeding approaches

In fact, the rectangular waveguide feed approach has been used in an early stage to succesfully develop a static leaky-wave antenna prototype based on NRD waveguide based on a teflon dielectric. This approach however proved to be inadequate when

trying to modifiy the prototype for inclusing of liquid crystals in a foam container. The container (being electromagnetically invisible, $\epsilon_r = 1$ prevents a smooth transition from rectangular guide to NRD.

It is desirable to directly launch the wave into the liquid. A coaxial launcher penetrating the LC container fulfills this necessity. In addition, they are readily available as standardized components and can be directly connected to a VNA, allowing for easy prototyping.

feed	excitation	size
coax	directly into LC	small
rect. guide	poor transfer → spurious radiation	bulky → platform needed

Table 3.3: Feed considerations

Frequency The unlicensed band around the 60GHz-frequency has been targetted. The choice results from the necessity of a relatively high frequency for better LC-performance. In addition, this band is promising for its applications in point-to-point communication such as HDMI high datarate video broadcasting.

3.4 Prototyping & Mechanical considerations

Two prototypes have been constructed that have been attemped to fill with LCs (Both attempts have taken place at the Technical University of Darmstadt, Germany in February and September 2013 respectively):

1. Rectangular waveguide feeding NRD from front (prototype developed at Fraunhofer FHR, Germany) (fig. 3.5)
2. Coaxial injection from the bottom (prototype developed at Delft University of Technology).

In both cases it has been attempted to contain the LCs within a Rohacell foam container (fig. 3.4) by injecting them with a siringe through the foam. Glue has been used to close the remaining hole. Unfortunately it has not been possible to keep the liquid confined within the structure and measurement results have proven to be useless.

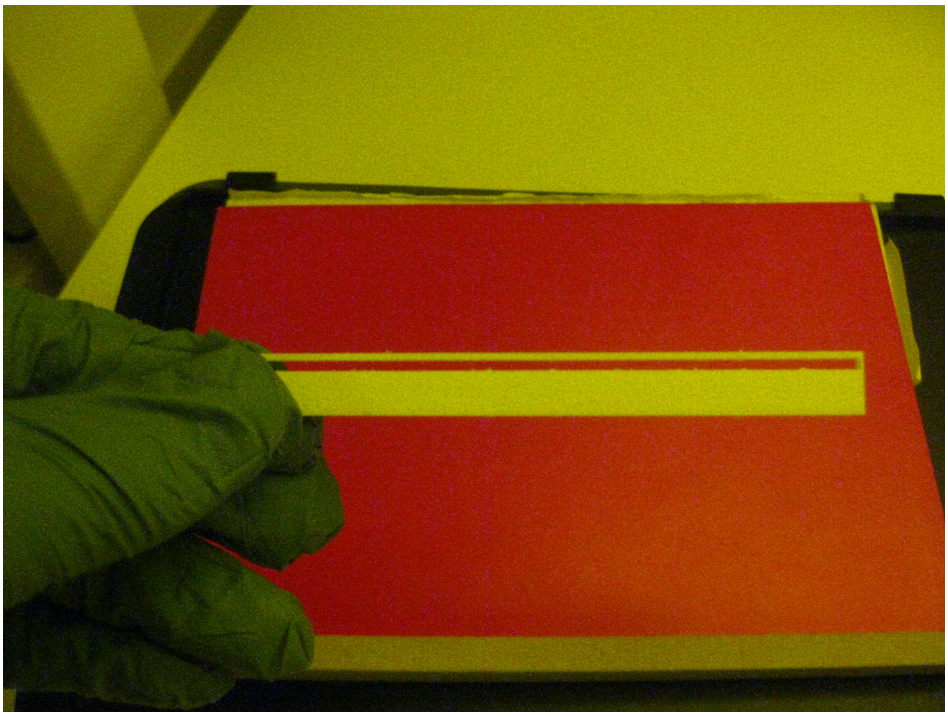

Figure 3.4: Photo of the used foam Rohacell container

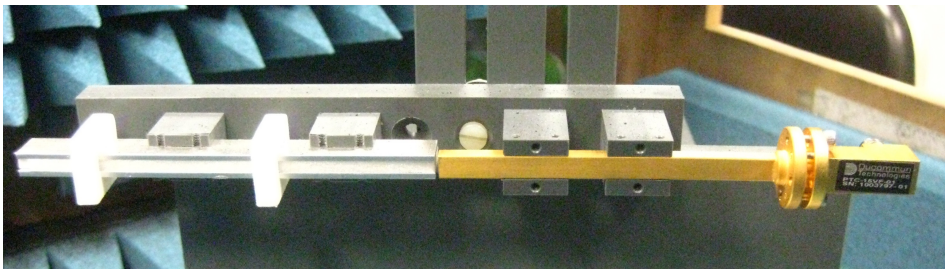

Figure 3.5: Rectangular waveguide-fed NRD mounted in measurement box

Waveguide analysis 4

4.1 Introduction

The antenna structures proposed in chapter 3 will be made specific in the upcoming chapter. More specifically, the structure's geometric parameters such as cross-section (a, b), length (l) and feed position will be determined.

Parameters The same common parameters will be assumed for the symmetric and asymmetric structure (with the obvious exception of feed position). This allows for fair mutual comparison later on. The determined parameters (that have been visualized in Figure 3.1) and values are listed in table 4.1.

Structure-specific parameters	Value (mm)	Variables	Value
Dielectric width, height (a, b)	2.00, 2.04	Frequency (f)	$59 \rightarrow 66$GHz
Gap size (d)	0.5	Dielectric (ϵ_r)	$2.6 \rightarrow 3.0$
Structure length (l)	180		
Coaxial insertion length (l_{ci})	0.9		

Table 4.1: Structure specific parameters and variables

Design objective There exists no design specification on which this antenna study is based. However it is necessary to set some basic design constraints to arrive at the parameters as shown in the table above:

1. The beam direction corresponding to the center operating point $(\epsilon_r, f_0) = (2.8, 62.5\text{GHz})$ is arbitrarily set at $\theta_m = 45°$
2. Most leaky-wave antennas are between $10\lambda_0$ and $20\lambda_0$ in size. Therefore, an upper lenght is aimed for: $l < 20\lambda_0$
3. The common rule of thumb as aimed for as maximally allowed input reflection: $S_{11} < -10$dB.

A three-step strategy is assumed in deriving the common and specific parameters:

1. Assumption of reasonable initial values (section 4.2).
2. Derivation of design space from constraints: desired operating point (f_0, ϵ_{r0}), beam angle (θ_0) and input reflection (S_{11}) (section 4.3).
3. Trade-off discussion and parameter choice (section 4.3).
4. Specific parameter determination, i.e. the asymmetric feed position is dealt with in section 4.4

4.2 Common parameter initialization

The parameter values for antenna structure length (l), gap size (d) and coaxial insertion length (l_{ci}) will be initialized. Structure length (l) is assumed to include the full structure on both sides of the (center) feed.

length (l) Most uniform leaky-wave antennas are up to 20 free-space wavelengths (λ_0) in size. This value has been chosen with the consequential length (l) rounded off: $l = 20 \cdot \lambda_0 = 20 \cdot \frac{f_0}{c} = \frac{62.5\text{GHz}}{3e8m/s} = 96\text{mm} \approx 100\text{mm}$.

gap size (d) The gap size should be electrically (very) small due the evanescant field. For this reason, a gap size of approximately 1/10th of a free-space wavelength (λ_0) has been selected as initial value: $d = \frac{1}{10}\lambda_0 = \frac{1}{10} \cdot \frac{f_0}{c} = 0.48\text{mm} \approx 0.5\text{mm}$[1].

insertion length (l_{ci}) The coaxial insertion length has been initialized by simulating a radiating coaxial probe (fig. 4.1) and varying the length of the unshielded part with the background dielectric having the dielectric constant of the liquid crystal. Coaxial dimensions are given in section 3.2. Input reflection for both freespace ($\epsilon_r = 1$) and dielectric background ($\epsilon_r = 2.8$) are shown in Figure 4.2. The coaxial insertion length (l_{ci}) has been therefore set at $l_{ci} = 0.9\text{mm}$.

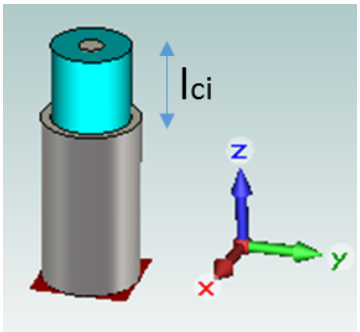

Figure 4.1: Full-wave solver model of free-standing radiating probe (input port shown in red).

[1]Note that the gap size (d) cannot be made arbitrarily small since in practice it is realized by solid foam (chapter 3).

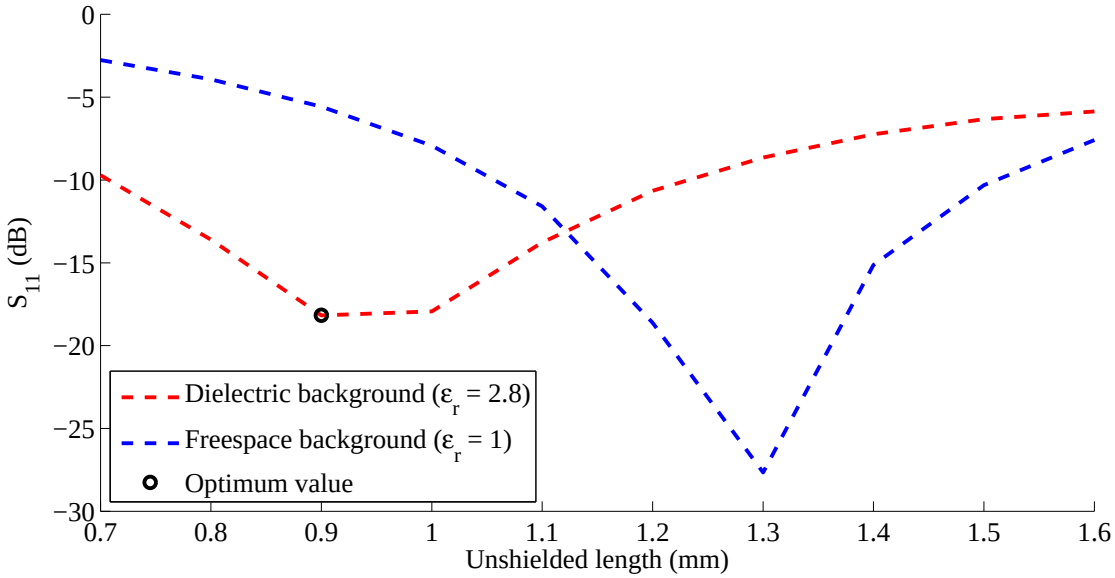

Figure 4.2: Input reflection of a free-radiating coaxial probe ($f_0 = 62.5\text{GHz}$)

4.3 Common parameter determination: cross-section, length, feed dimensions

The parameters (a, b, l) shall be determined simultaneously[2] in three steps (and be based on the design constraints mentioned previously):

1. Design space reduction.
2. Quantification of design trade-off.
3. Determination of (a,b,l).

The steps above will performed using the symmetric structure as basis.

4.3.1 Design space reduction

It shall now be demonstrated how the continuum of (a, b)-values is reduced to a discretized set: (a, b) will be chosen such that the phase constant (β) inside the waveguide will assume a value that results in desired radiation (θ_0) outside. Phase constant (β) can be found by rewriting equation (2.4) that links it to beam direction as has been done in (4.1).

$$\beta = k_0 \cdot \cos\theta_0 = \frac{2\pi f}{c} \cdot \cos\theta_0 = 925\text{m}^{-1}\,(f = 62.5\text{GHz}, \theta_0 = 45^\circ) \tag{4.1}$$

It is necessary to find combinations of dielectric cross-section (a, b) that allows for excitation and support of a wave with the phase constant β mentioned above. To this

[2]Simultaneous determination is needed since a particular choice for (a, b) influences the required length (l) and vice versa

end the full-wave solver has been used to find the desired mode (based on a closed structure) and find the (a, b)-values that correspond to the required phase constant β. Three modes have been considered here: quasi TEM, hybrid (dominant horizontal E-field), hybrid (dominant vertical E-field). The corresponding modal patterns can be found in Appendix C.

it is necessary to excite a so-called fast wave ($\beta < \beta_0$), i.e. a higher order non-TEM mode, in order to provide radiation. The two hybrid modes fulfill this criterion, of which one in particular turns out to be excited rather well by the coaxial excitation. This mode has been shown in Figures 4.3, C.1c and C.2c. Here it can be seen how the top and bottom boundaries are modelled as perfect magnetic conducting (PMC) to approximate the air interface.

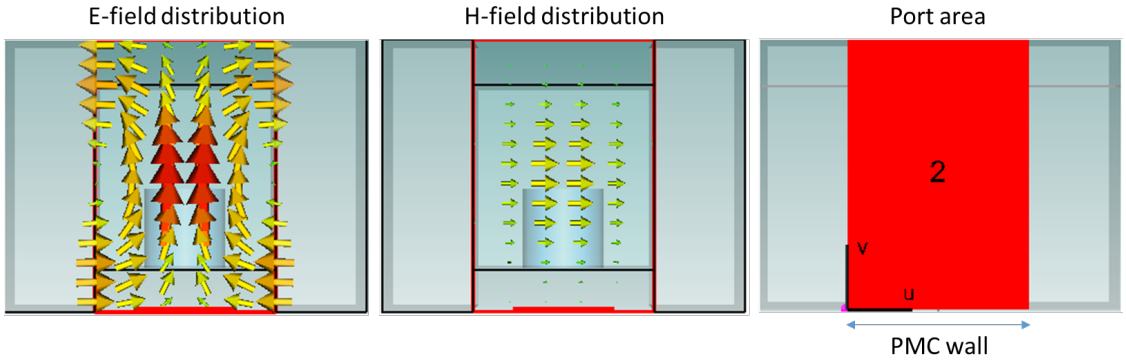

Figure 4.3: Closed structure desired mode field distributions

An infinite set of combinations of (a, b)-values results in the desired phase constant (β) for the closed structure mode[3]. A finite subset for which $\beta = 925\text{m}^{-1}$ has been computed by the full-wave solver and is displayed in Table 4.2[4].

Dielectric width (a) (mm)	1.8	1.9	2.0	2.1	2.2	2.3
Dielectric height (b) (mm)	2.83	2.34	2.04	1.82	1.66	1.52

Table 4.2: Dielectric dimensions width (a) and height (b) that result in the desired phase constant β

4.3.2 Quantification of design trade-off

Before proceeding to make a choice for the (a, b, l)-triad the parameter choice trade-off will be made insightful. To this end the following quantities will be computed as a function of (a, b) for the initial parameters as derived in Section 4.2 and where $f_0 = 62.5\text{GHz}$:

[3]Here it is assumed that opening the closed structure (i.e. assuming a small value for gap size (d)) does not alter the phase constant drastically

[4]In fact, the actual mode computation has been performed for very large air gap (d) values. For sake of clarity the computed field distributions are shown with a small gap size

1. $k_z = \beta - j\alpha$
2. input reflection S_{11}
3. minimal required length (l_{min})

k_z The wavenumber k_z is computed by simulating the (dominant) vertical electrical field E_y along one half of the longitudinal (z-)axis in the center of the dielectric for each (a,b)-combination listed in Table 4.2. Then, it is necessary to decompose the aggregate waveform in terms of decaying complex exponentials in order to extract the leaky waves. To this end the Matrix-Pencil (MP) method has been employed. This algorithm takes as input the simulated data for E_y and outputs complex poles z_i and corresponding weighing coefficients R_i from which a leaky wavenumber $k_{z,i}$ and a corresponding decaying exponential waveform can be constructed (see also Appendix B).

This approach will now be illustrated for $(a, b) = (2.0\text{mm}, 2.04\text{mm})$. Symmetric feeding is assumed and half of the waveguide will therefore be of interest. The field is evaluated over a range of 50mm and a sample step size of $\Delta X = 0.25\text{mm}$ as has been illustrated in Figure 4.4.

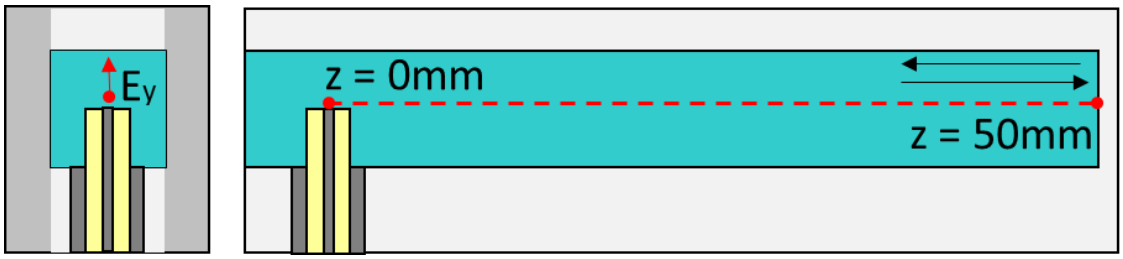

Figure 4.4: Evaluation range of E_y (note that only the right half of the symmetric structure is shown)

The resultant aggregate waveform is shown in Figure 4.5a. Applying the MP-method results in decaying exponentials shown in Figure 4.5b. Clearly, two components correspond to a forward and reflected leaky-wave. These sum of these two components forms the approximation shown in Figure 4.5a.

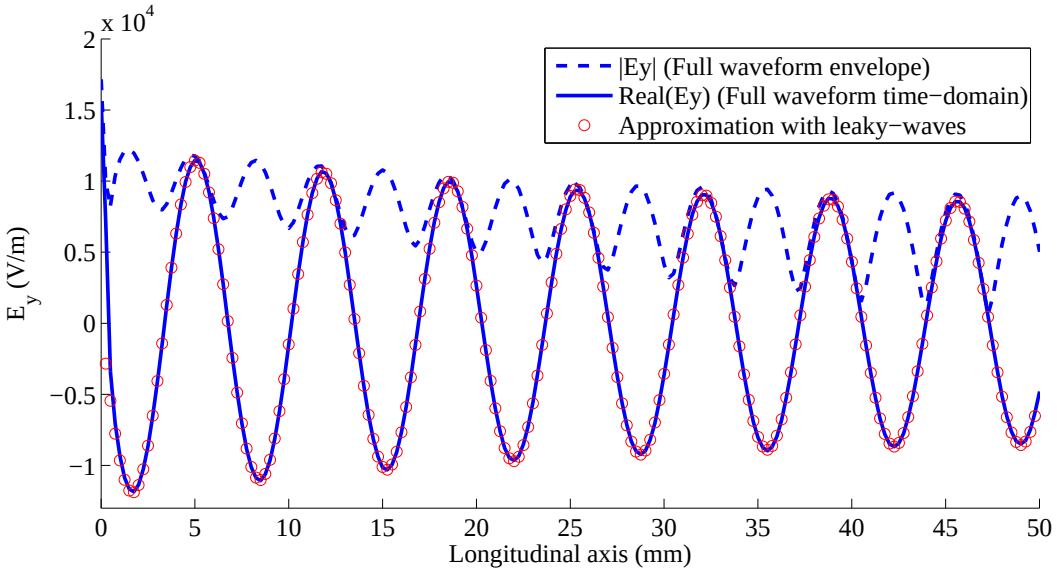

(a) Aggregate waveform and leaky-wave approximation

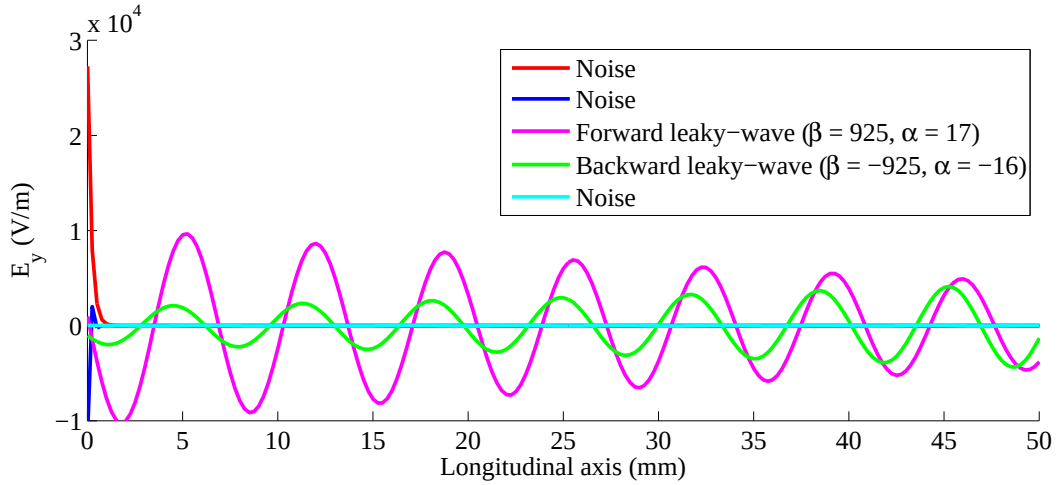

(b) Decomposition individual components

Figure 4.5: Application of Matrix-Pencil method explained

The method described above has been applied repeatedly to simulations of structures with different dielectric cross-sections (a, b) and tuning states (ϵ_r). The excited leaky-wave numbers $k_z = \beta - j\alpha$ have been computed in a similar manner to the example shown in Figure 4.5b and are shown in Figure 4.6 as a function of (a, b) (and tuning state ϵ_r) for $f_0 = 62.5$GHz.

The computed values of k_z are used for the final length determination for the determination of the antenna's aperture length l at the end of this section.

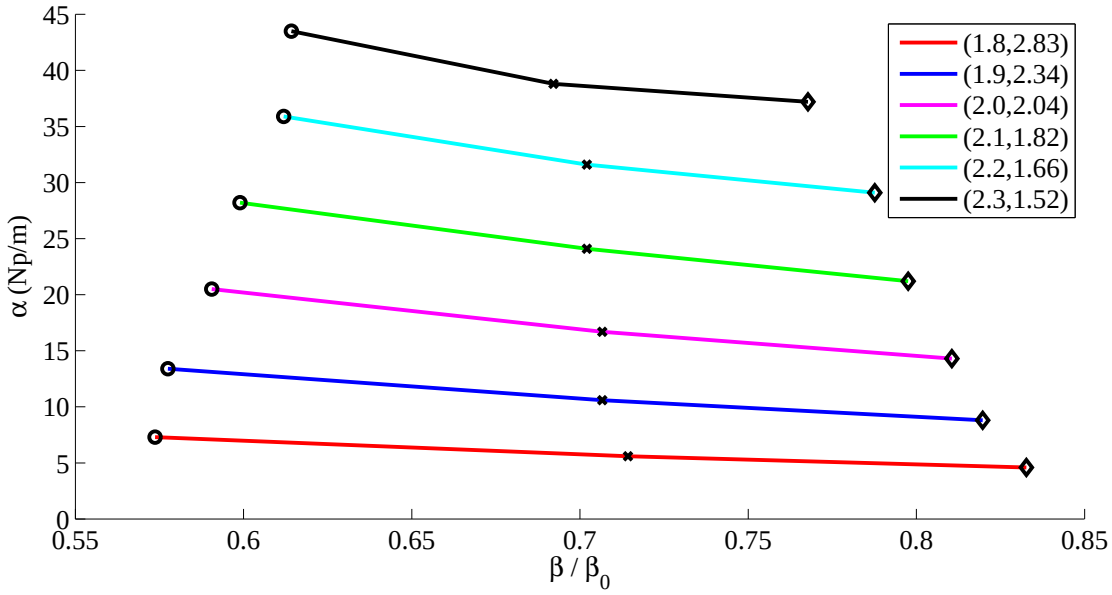

Figure 4.6: k_z as function of (a, b) and tuning states $\epsilon_r = 2.6$ ($\circ$), $2.8(x)$, $3.0(\diamond)$

S_{11} The behavior of S_{11} as a function of (a,b) can be illustrated by distinguishing between a finite and an infinite structure. The latter can be simulated by placing an absorbing port at the structure's ends. Ideally, if enough energy has left the structure the S_{11}-graphs should coincide.

Furthermore, it is desirable to aggregate S_{11}-behavior into a single quantifier. To this end, S_{11} has been both computed for the center frequency (62.5GHz) as well as averaged over the full band. The results are displayed in Figure 4.7.

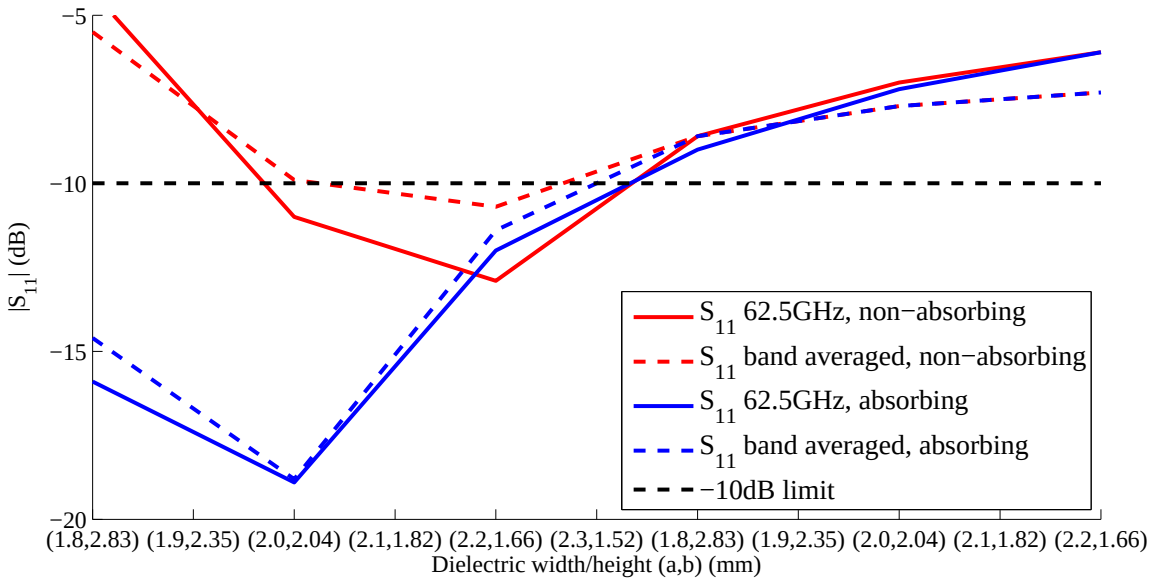

Figure 4.7: Input reflection (S11) vs. (a,b) for $f_0 = 62.5$GHz

One can observe that matching improves for narrower structures for the infinite structure. For wider structures however, matching is cumbersome, presumably due to the increasing proximity of the dielectric top wall to the coaxial probe. The finite structure on the other hand shows a discrepancy for the narrower dielectric sizes. This can be explained by unradiated energy reflected back from the end of the structure into the input probe.

l_{min} The total antenna aperture length l will now be determined. The required minimal length of the entire antenna structure is a function of the leakage-rate α and the desired radiation efficiency η. The radiation efficiency of a uniform leaky-wave antenna is given in [18] is equal to (4.2) where l_{ap} is the aperture size and rewriting as a function of aperture size results in (4.3).

$$\eta = 1 - e^{-2\,\alpha l_{ap}} \tag{4.2}$$

$$l_{ap} = \frac{\ln(1-\eta)}{-2\alpha} \tag{4.3}$$

Since calculations are based on the symmetrical antenna with center feeding an additional factor of 2 needs to be included for the minimal required antenna length which is given in (4.4).

$$l_{min} > 2 \cdot l_{ap} = -\frac{\ln(1-\eta)}{\alpha} \tag{4.4}$$

If we assume an arbitrarily desired radiation efficiency η of 95% and include the attenuation constants for $\epsilon_r = 2.8$ from Figure 4.6, one can arrive at a graph displaying the minimal required antenna size as a function of dielectric cross-section (a, b). This graph is shown in Figure 4.8.

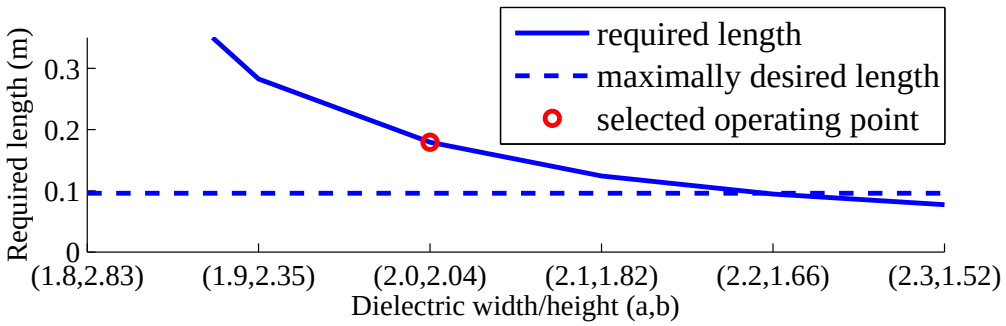

Figure 4.8: Required structure length vs. (a,b) for a 95 percent leakage of energy (5 percent remaining)

4.3.3 Establishing parameters based on trade-off

In the prevous section the design trade-off has been quantitively discussed. Ideally, a specific choice for the (a,b,l)-triad should be made based on the self-imposed design

criteria:

1. structure length: $l < 20\lambda_0$
2. input reflection: $S_{11} < -10dB$ (for f_c and average)
3. radiated energy: $\eta < 0.05$

From Figures 4.7 and 4.8 it can be seen that these requirements cannot be simultaneously met. Therefore, it is necessary to violate one of the design criteria: a larger structure length is selected. The minimal extra length is required for (a,b) = (2,2.04). For (a,b) = (2.0,2.04), assuming a required 95 percent of radiated energy a minimum length is required of 179.4mm using a value of $\alpha = 16.7\text{m}^{-1}$. Rounding off, the finalized structure length is established at $l = 180\text{mm}$

4.4 Specific parameter determination: feed position (asymmetric)

The position of the feed of the asymmetric structure (z_{fa}) needs to be established. Aiming to exploit the principle of constructive interference, it can be assumed that several candidate positions z_{fa} exist (Figure 4.9). A choice will be made on the quality of the resultant radiation pattern and input reflection.

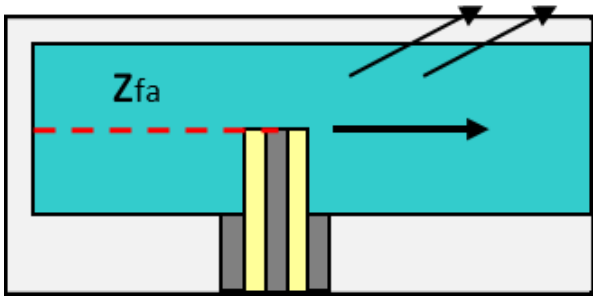

Figure 4.9: Determination of asymmetric feed position z_{fa}

An initial test simulation has been performed by placing the feed two guided wavelengths away: ($z_{fa} = 2 \cdot \lambda_z$)[5]. The (normalized) electric E_y field is shown in Figure 4.10 where it has been decomposed in terms of decaying exponentials corresponding to leaky waves by again using the MP-method.

The following observations can be made based on the field decomposition in Figure 4.10.

1. The desired (leaky) wave ($\beta = 925\text{m}^{-1}$) is excited in the forward ($z > z_{fa} = 13.6\text{mm}$) region (as the sum of a direct and reflected wave).
2. An undesired (leaky) wave ($\beta = 1200\text{m}^{-1}$) is excited in the forward ($z > z_{fa}$) region (possibly by the reflected wave impinging on the feed)

[5]For the desired leaky-wave phasconstant ($\beta = 925\text{m}^{-1}$) this corresponds to $2\lambda_z = 13.6\text{mm}$

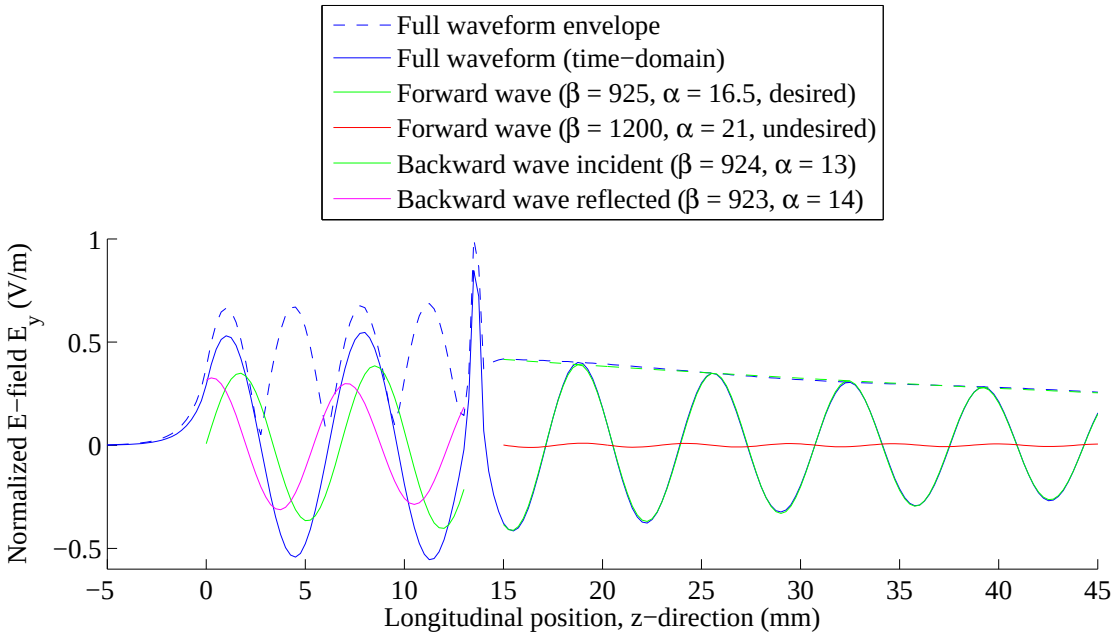

Figure 4.10: Wave decomposition E_y for asymmetrical feed (source positioned at $z_{fa} = 13.6\text{mm}$)

3. The left-end wall ($z = 0\text{mm}$) does not behave as a perfect open but adds an additional phase shift ($\Delta\phi$) to the reflected wave. This can be concluded from the envelope maximum at $z = z_0 \approx 1\text{mm}$ instead of $z = 0\text{mm}$.

It is hypothesized that by moving the feed location z_{fa} to one of the maxima of the full waveform envelope, the forward wave (green) and reflected wave (magenta) will add up in phase for ($z > z_{fa}$), i.e. for $z_{fa} = z_0 + n \cdot \frac{1}{2}\lambda_z$[6], where z_0 is the offset due to the additional phase shift $\Delta\phi$ from ther reflection. Likewise, some sense of destructive interference is to be expected for feed positions at $z_{fa} = z_0 + \frac{1}{4}\lambda_z + n \cdot \frac{1}{2}\lambda_z$[7].

Therefore, simulations have been performed to compute input reflection (S_{11}) and (realized) gain[8] as a function of feed position. More specifically, S_{11} has been computed for both center frequency f_0 as well as band averaged in Figure 4.11.

It is interesting to note that both input reflection S_{11} (for f_0) and gain (and importantly directivity!) increase and decrease when the feed is moved along mentioned positions of maxima and minima. The band avaraged reflection however gradually decays with position. This is to be expected since a feed that is positioned further away from the wall will already have lost some energy in the section left of the feed ($z < z_{fa}$).

From the gain/directivity-plot in Figure 5.2 it can be further observed that the intensity of the undesired beam fluctuates. Because the gap between desired and undesired beam gain is largest at $z_{fa} = 7.8\text{mm}$ this value has been chosen as the final feed position.

[6]Maxima corresponding to $z_{fa} = 1.0\text{mm}, 4.4\text{mm}, 7.8\text{mm}$

[7]Minima corresponding to $z_{fa} = 2.7\text{mm}, 6.1\text{mm}, 9.5\text{mm}$ ...

[8]The gain is associated withantenna performance and therefore displayed in Chapter 5

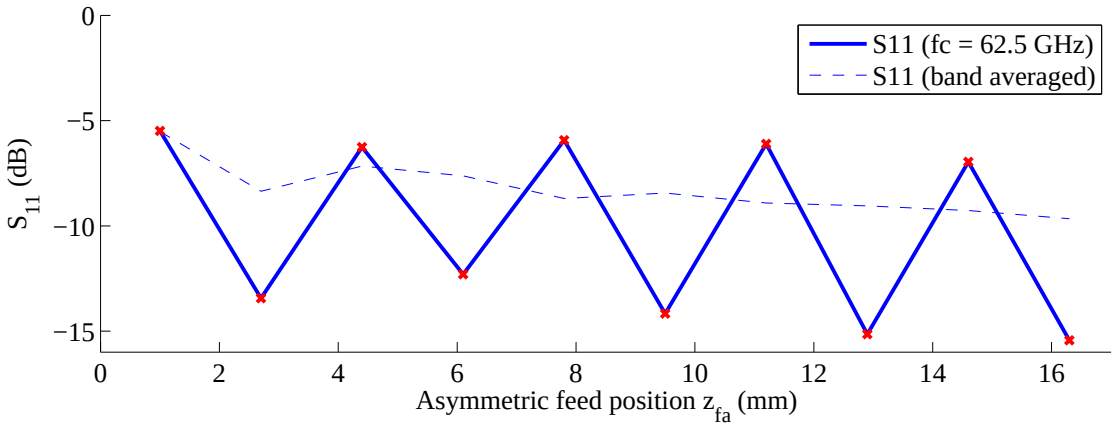

Figure 4.11: S_{11} behavior as a function of feed position

4.5 Conclusion

Waveguide analysis has been performed resulting in parameter determination for both the symmetric and asymmetric structure.

Parameters of both the symmetric (and thereby the asymmetric) have been determined based on a set of self-imposed design constraints with respect to input reflection, aperture length and radiation efficiency. Unfortunately it has been necessary to violate the criterion on maximum antenna length, extending the structure length l from 100mm to 180mm.

Furthermore, the desired position of the asymmetric feed has been established based on value of the corresponding antenna gain and the amount of suppression of the unwanted excited mode.

5 Leaky waveguide radiation

5.1 Introduction

This chapter presents the antenna characteristics associated with the leaky-wave antennas derived in the previous chapters.

5.2 Asymmetric: Gain & input reflection (S_{11}) vs. feed position

The gain and input reflection has been computed as a function of feed position. This has been done to perform the feed position (z_{fa}) determination as has been done in section 4.4.

In fig. 5.1a a gain-vs-theta plot is shown for a few (z_{fa}) values in fig. 5.1a in which the beams associated to the excited desired and undesired modes can be seen[1]. A rigorous plot illustrating the dependence with the feed position (z_{fa}) is shown in fig. 5.2.

Observations from fig. 5.1a and fig. 5.2:

1. The periodic nature of the directivity plot indicates the constructive/destructive interference phenomenon when placing the feed in a node/anti-node (as discussed in section 4.4).
2. The undesired mode exciation shows no periodic behavior. Therefore periodic causality with (longitudinal) feed position cannot be proven.
3. The maximum gap between desired/undesired mode is found for $z_{fa} = 7.8$mm, hence the parameter choice in section 4.4

[1]The desired and undesired modes correspond to a beam around 45°and 23°respectively

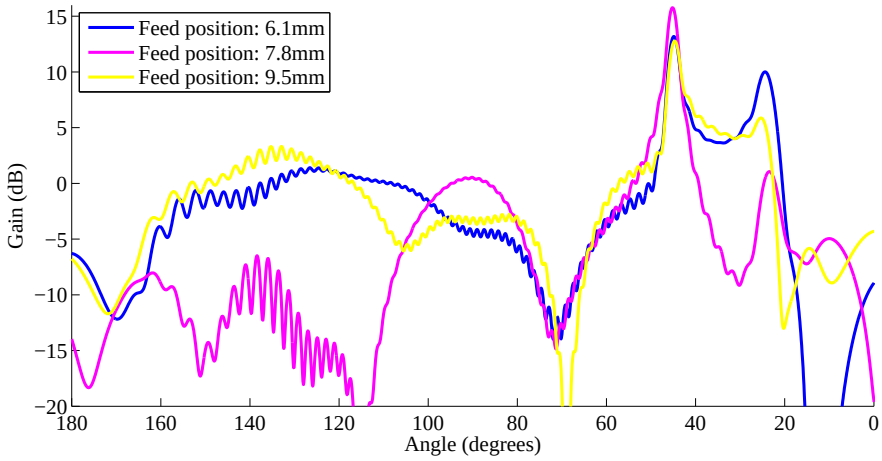

(a) Gain vs. angle for several feed positions ($z_{fa} = 6.1\text{mm}, 7.8\text{mm}, 9.5\text{mm}$)

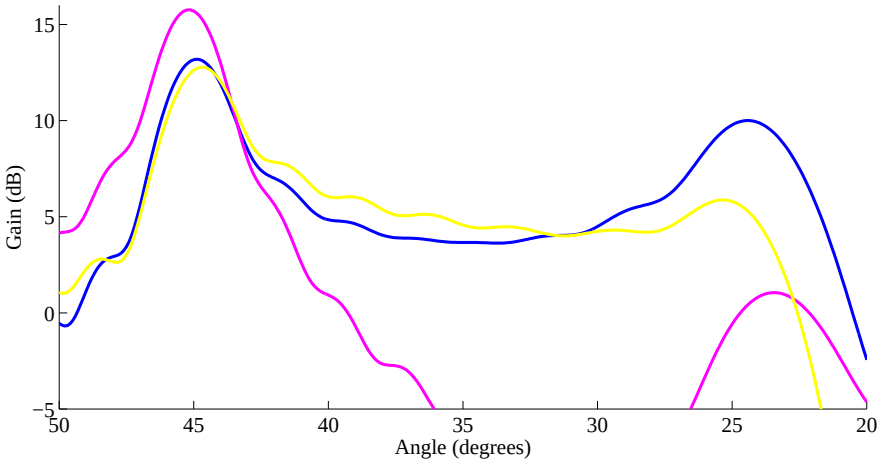

(b) Close-up around beam maxima

Figure 5.1: Asymmetric structure gain behavior for several feed positions

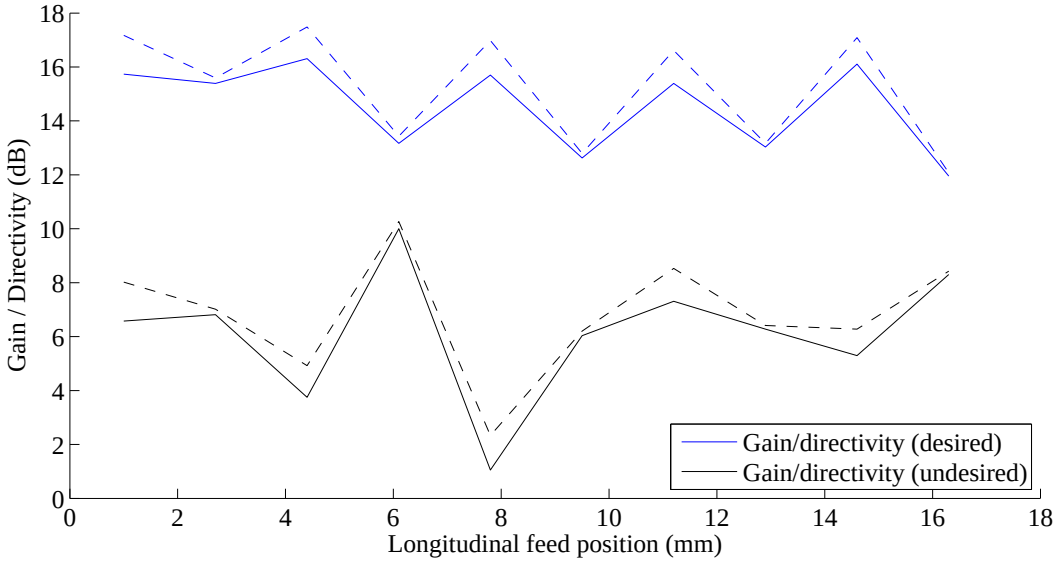

Figure 5.2: Maximum directivity (dashed) / gain (solid) vs. feed position

5.3 Symmetric & asymmetric: Gain and S_{11} vs. tuning state (f_c, ϵ_r)

In this section the characteristics of both antenna structures will be studied in which two steps can be distinguished:

1. Qualitative analysis of the far-field pattern for the operating point: f_0, ϵ_{r0}.
2. Quantitative analysis of gain (G), input reflection (S_{11}) and bandwidth behavior around the operating point: $59\text{GHz} < f < 66\text{GHz}$, $2.6 < \epsilon_r < 3.0$.

5.3.1 Qualitative analysis

Far-field gain computation for both structures has been performed and is displayed in fig. 5.3 (3D) and fig. 5.4a(2D, $\phi = 90°$).

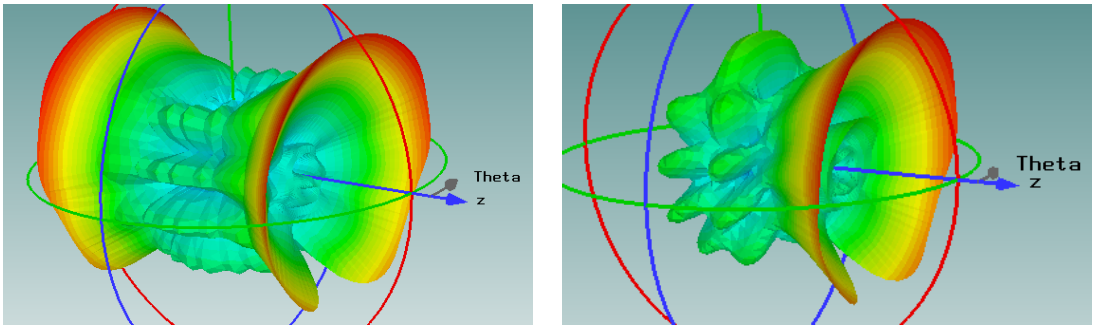

(a) Symmetric feed (b) Asymmetric feed

Figure 5.3: Qualitative (3D) radiation pattern

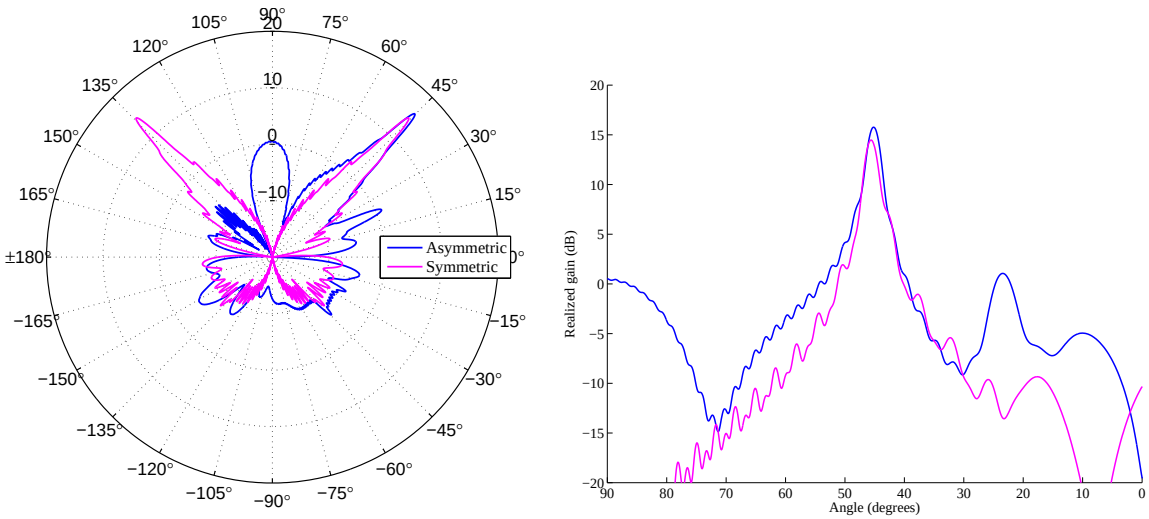

(a) Polar plot (b) Close-up of 0° to 90°

Figure 5.4: Quantitative (2D) radiation pattern ($\phi = 90°$) for $(f_0, \epsilon_{r0}) = (62.5, 2.8)$

The following observations can be made:

1. A double or single fan beam is excited indicating succesful implementation of an ideal line source designed for $\theta_0 = 45°$.
2. The asymmetric structure features a higher beam intensity due to larger aperture and constructive interference (see fig. 5.4a).
3. The symmetric structure features a clean pattern whereas the asymmetric displays an undesired lobe at broadside ($\theta = 90°$) and $\theta = 23°$ (section 5.2).

Summarizing, the chosen type of waveguide (NRD) behaves as a good approximation of an ideal line source for both the symmetric and asymmetric feeds.

5.3.2 Quantitative analysis

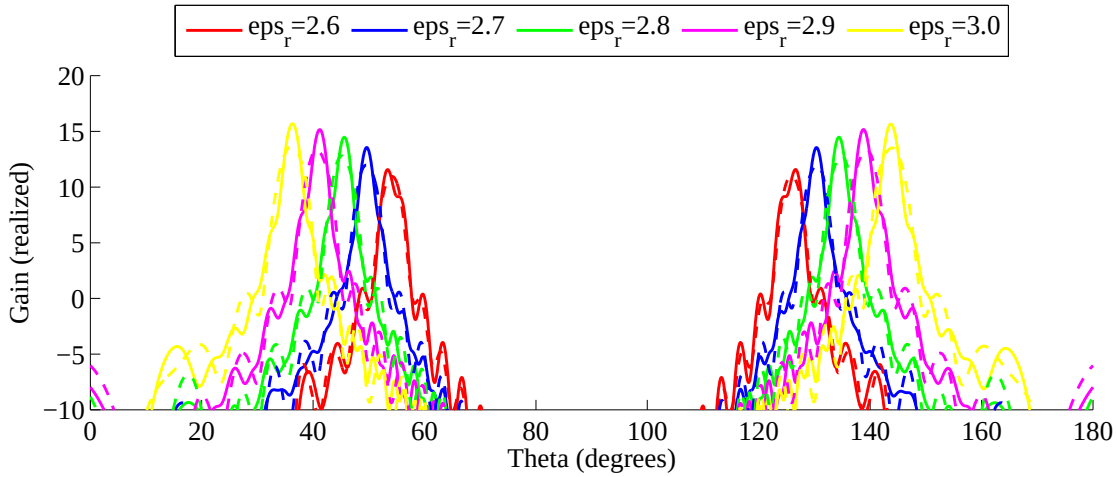

(a) Symmetric feed (solid/dashed = non-absorbing/absorbing)

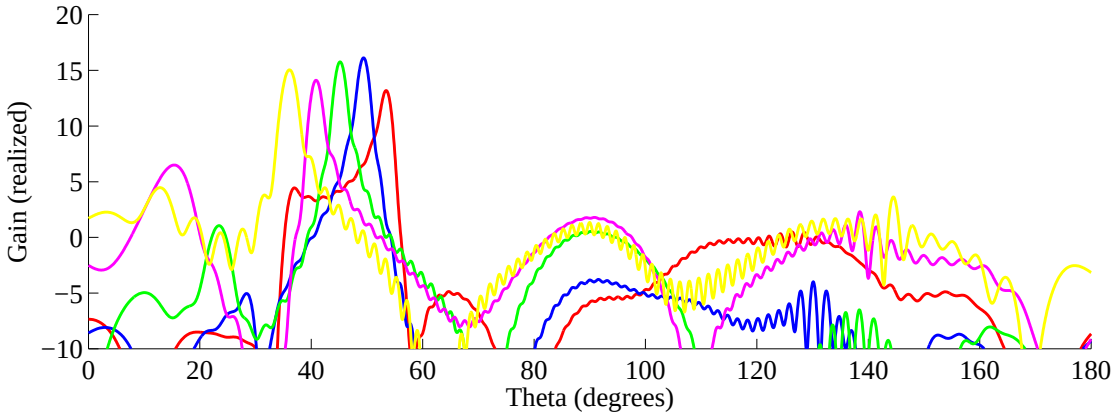

(b) Asymmetric feed

Figure 5.5: Far-field gain for different tuning states of ϵ_r ($\phi = 90°$)

The quality of the radiation patterns for different tuning states ϵ_r are shown in fig. 5.5, summarizing:

1. The symmetric structure features a clean pattern where only the desired mode is excited corresponding to a single beam.
2. The asymmetric structure features unwanted mode excitation: the intensity of the desired beam does not show a smooth transition between different tuning states (energy is divided between desired and undesired mode).
3. The symmetric structure shows discrepancy between beams with and without absorbing port: energy is reflected from the end of the structure resulting in interference with the "other" beam.
4. Consequently, the beam with highest leakage ($\epsilon_r = 2.6$) shows most similarity between absorbing/non-absorbing structure.

5.3.3 Full antenna reconfiguration behavior for $2.6 < \epsilon_r < 3.0$ and $59\mathbf{GHz} < 62.5\mathbf{GHz} < 66\mathbf{GHz}$

To gain insight in the overall quality of the antenna structures the maximum gain (fig. 5.6), associated maximum gain angle θ_m (fig. 5.7), input reflection (fig. 5.8) and (-3dB) bandwidth (fig. 5.9) are computed for both antenna structures and each possible tuning state (ϵ_r, f_0). The resulting color matrices can be considered a reconfiguration table, displaying the full aggregate of antenna features.

Gain Two features of the gain matrices (fig. 5.6) are striking. The first is that so-called areas of higher antenna gain are found in the lower right corner corresponding to either a high frequency, a high dielectric constant or both. This makes sense because of the relatively low attenuation α of the excited leaky wave, resulting in a sharper beam.

The second feature to note is the smooth gain transition for the symmetric structure whereas the asymmetric structure shows a rough transition. This can be explained by the seemingly random distribution of energy between the so-called desired and undesired leaky modes as could already be observed in figs. 4.10, 5.1a and 5.5b.

Angle The angle-matrices (fig. 5.7) show the direction of maximum gain. As it can be expected the figures look quite similar for both structures. This is not surprising the the excited leaky waves should at least theoretically have the same wavenumber k_z as both structures have the same cross-section. The minor discrepancy that does exist are the few light blue spots in upper left corner for the asymmetric angle matrix. These jumps can be attributed to the undesired mode suddenly becoming stronger than the desired one resulting in a sudden jump of maximum gain direction.

Input reflection (S_{11}) The antenna structures display a stark difference from the perspective of input reflection behavior as is observed in fig. 5.8. The symmetric structure shows decent matching over the full 60G-band for several tuning states ($\epsilon_r = 2.8$ and up). It is assumed this is the case since the situation is to some extent comparable to the freestanding radiating probe (fig. 4.2) that is now feeding the guide: there is very little reflection once the wave is launched. The asymmetric structure on the other hand suffers from a lot of additional reflection from the reflected wave, resulting in an extremely narrowband behavior. If the common -10dB design constraint would be applicable then this narrowbandedness seriously impairs freedom in antenna reconfiguration.

Bandwidth (-3dB) The beam squint that corresponds to a change in frequency of a leaky-wave antenna puts an upper limit on the operational bandwidth of each tuning state (ϵ_r, f_o): different frequency components will arrive at the receiver with different intensity.

To this end, the -3dB-bandwidth has been estimated for each tuning state in order to gain some sense of the possible operational bandwidths[2]. More specifically, this bandwidth is the amount Δf that the frequency can deviate from its operating point before the gain in the operating point's beam direction drops by 3dB.

A simple bandwidth estimation procedure has been followed. For each tuning state:

1. the 3dB *beamwidth bw* has been computed based on simulated gain data.
2. a so-called tuning rate r is computed representing the amount of scanned angle per hertz by comparing beam angle to the neighboring tuning state: $r = \frac{\Delta\theta}{\Delta f}$
3. bandwidth is consequently the ratio of beamwidth and tuningrate: $B = \frac{bw}{r}$

The results of these (automated) computations are shown in fig. 5.9. The symmetric bandwidth matrix is spotty in the top left corner which is unreliable since a smooth transition is to be expected. After investigation it turns out that radiation patterns associated to these tuning states with low dielectric constants and frequencies exhibit strange behavior such as multiple or split beams. The asymmetric bandwidth matrix shows more plausible (i.e. smooth) behavior, with the exception of the three blue dots that correspond to the undesired modes becoming dominant as has been discussed earlier.

A cautious estimation can be made that for the operable tuning states (lower right corner of the color matrices) a bandwidth of 800MHz is attainable, which comes down to a fractional bandwidth of roughly $\frac{0.8\text{GHz}}{62.5\text{GHz}} \approx 1.3\%$.

[2]Note that this does not relate to the bandwidth associated to input reflection

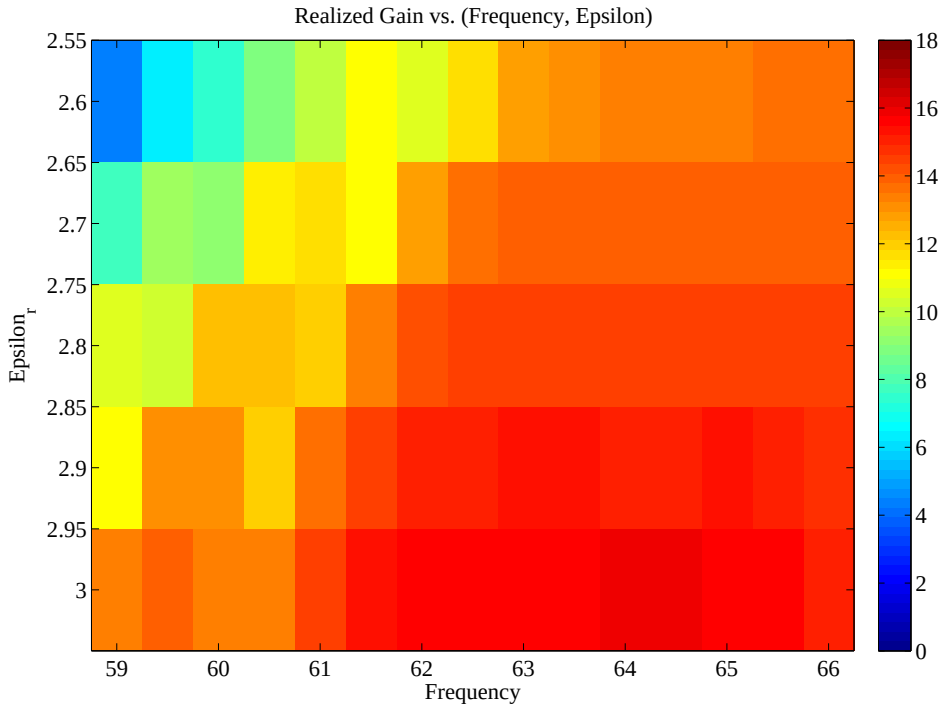

(a) Symmetric feed

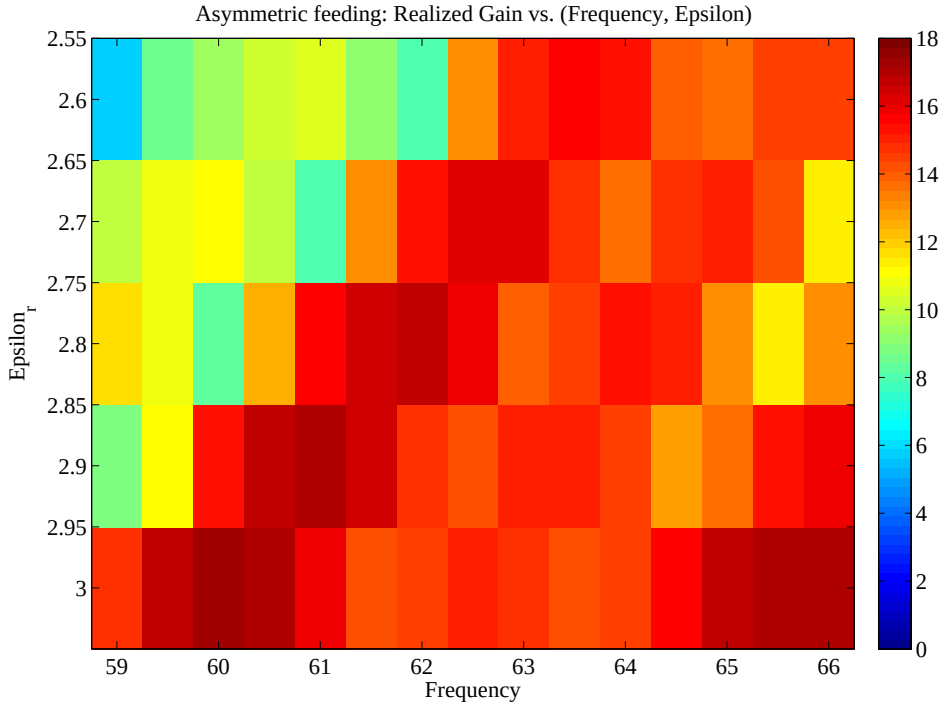

(b) Asymmetric feed

Figure 5.6: Realized gain vs. tuning state (ϵ_{r0}, f_c)

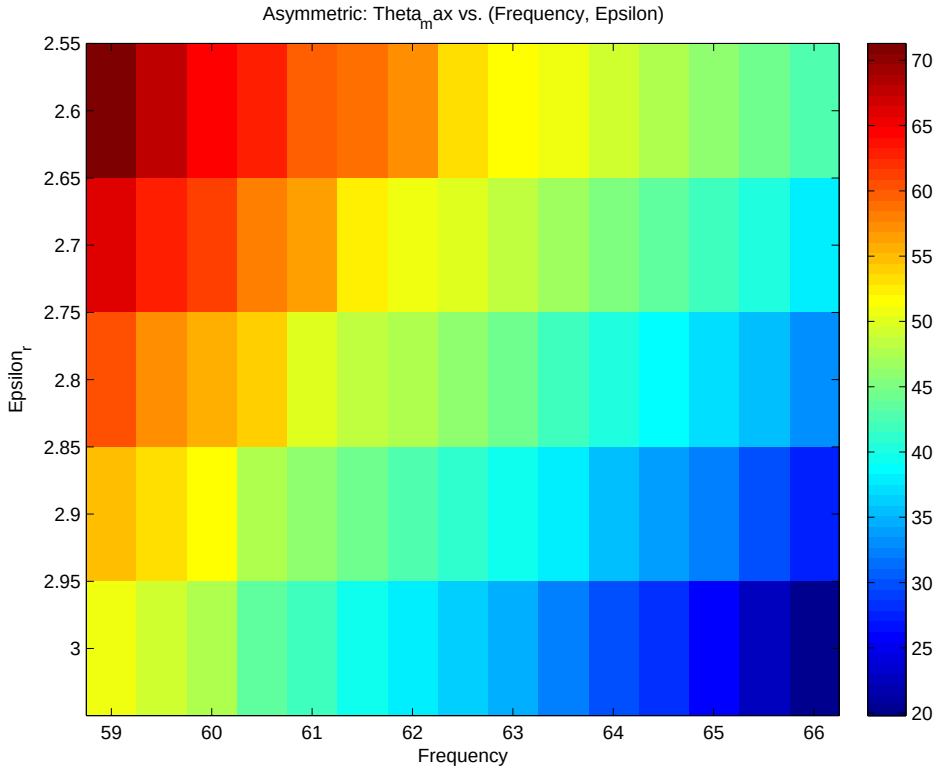

(a) Symmetric feed

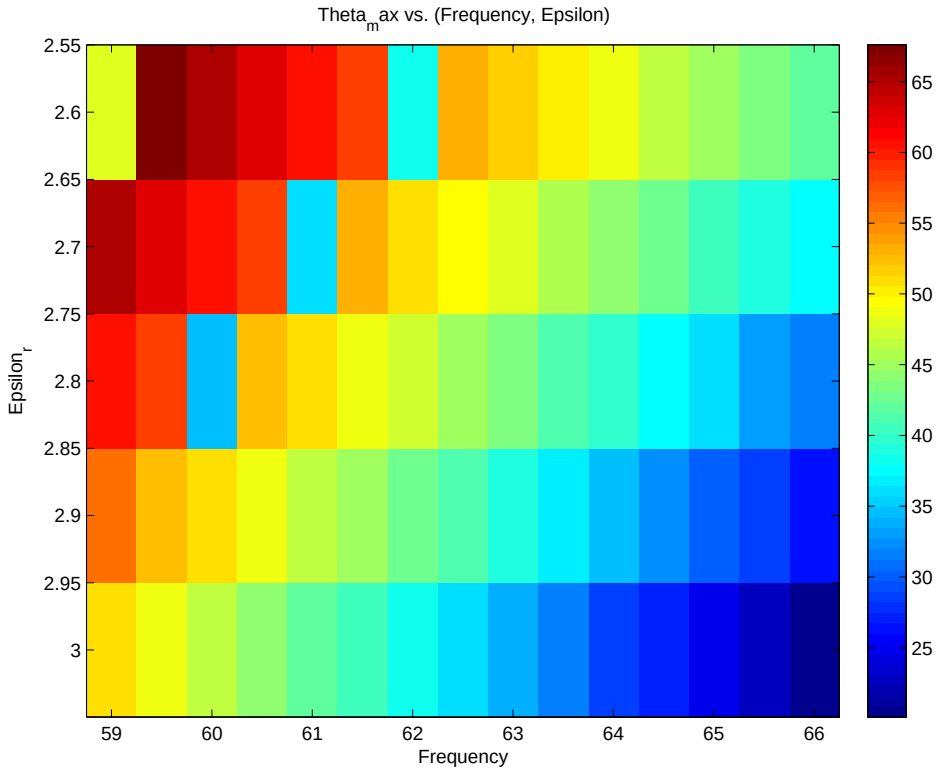

(b) Asymmetric feed

Figure 5.7: Maximum beam angle (θ_m) vs. tuning state (ϵ_{r0}, f_c)

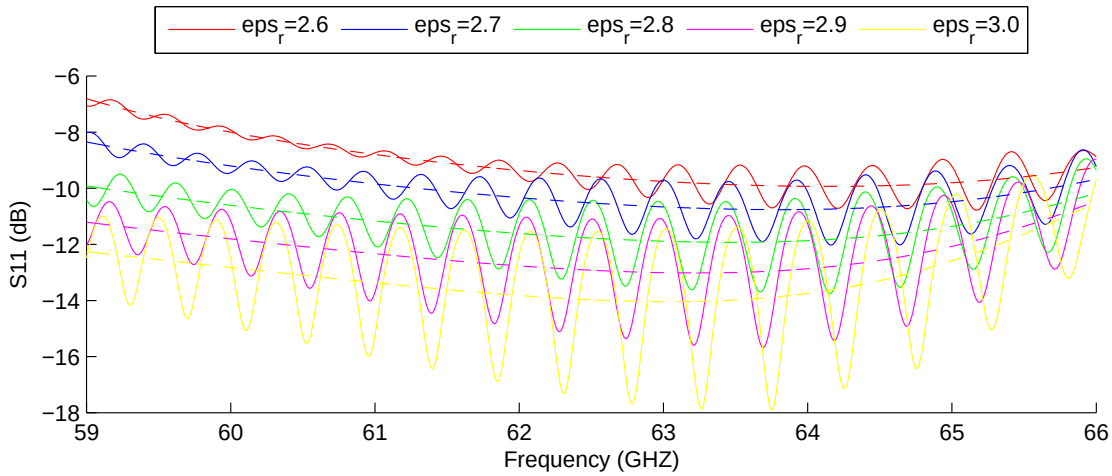

(a) Symmetric feed

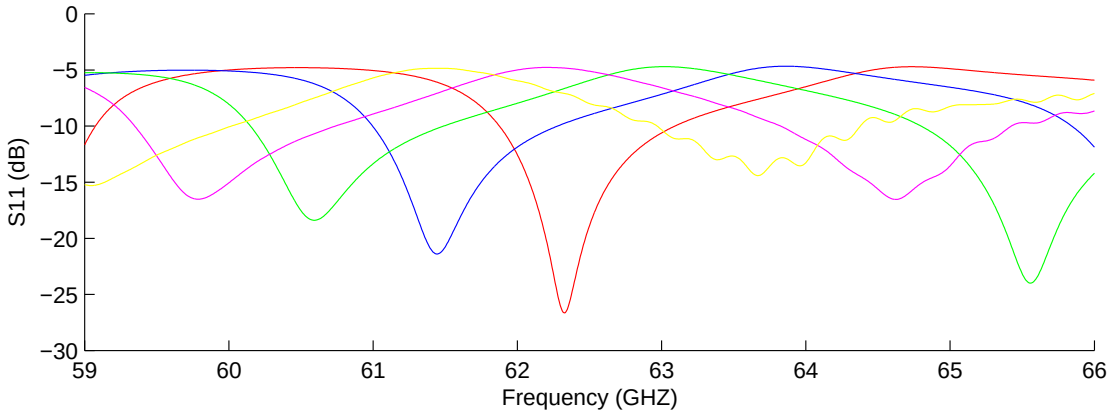

(b) Asymmetric feed

Figure 5.8: S_{11} vs. frequency per tuning state

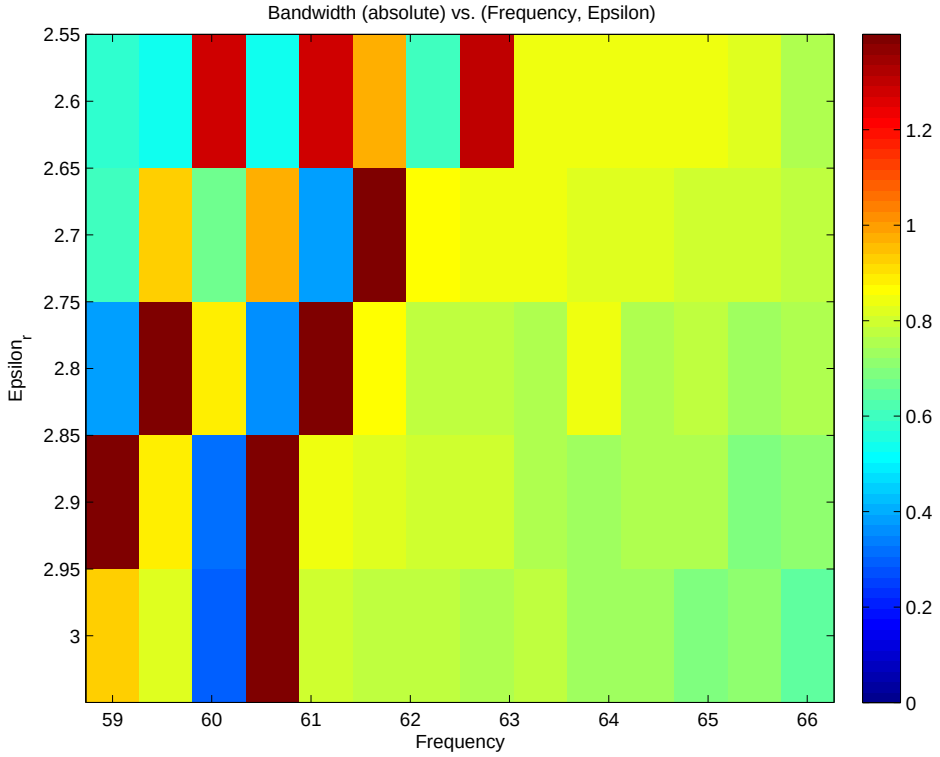

(a) Symmetric feed

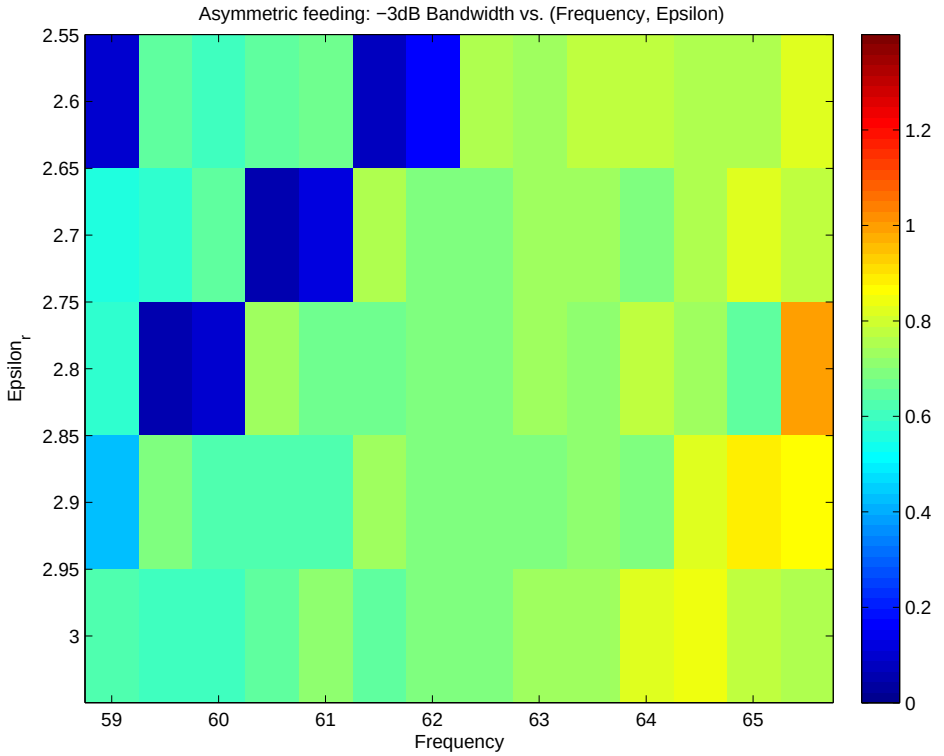

(b) Asymmetric feed

Figure 5.9: -3dB bandwidth matrix for each tuning state

5.4 Validation of theoretical model

It is insightful to compare the simulated far-field patterns with the theoretical model of a radiating line-source. The theoretical expression of the far-field has already been introduced in the beginning in (2.3). One half of the simulated far-field data of the symmetric structure shall be compared with this theoretical expression.

Input to this expression is the structures length (l) and the leaky-wave number (k_z). Length (l) has been established in chapter 4 as 180mm. Since we're considering half the radiation pattern a length l of 90mm is used for the line source. The leaky-wave numbers k_z have already been extracted in chapter 4 as well using the MP-method and repeated here below in graphical form (fig. 5.10).

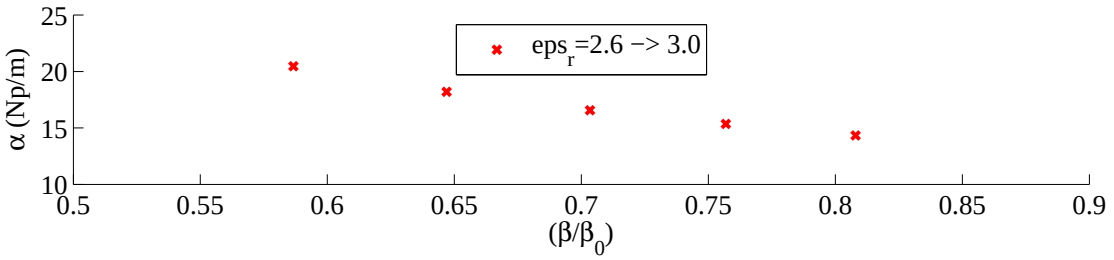

Figure 5.10: Leaky-wave number $k_z = \beta - j\alpha$ as function of tuning state ϵ_r

Normalization of both simulated and theoretical far-field pattern[3] results in a very nice comparison as shown in Figure 5.11. This leads one to conclude that for the principal plane, a (magnetic) current/line source is a very good model for this type of leaky waveguide.

[3]The theoretical far-field expression for $|E_\phi|$ has been squared to represent (normalized) energy density

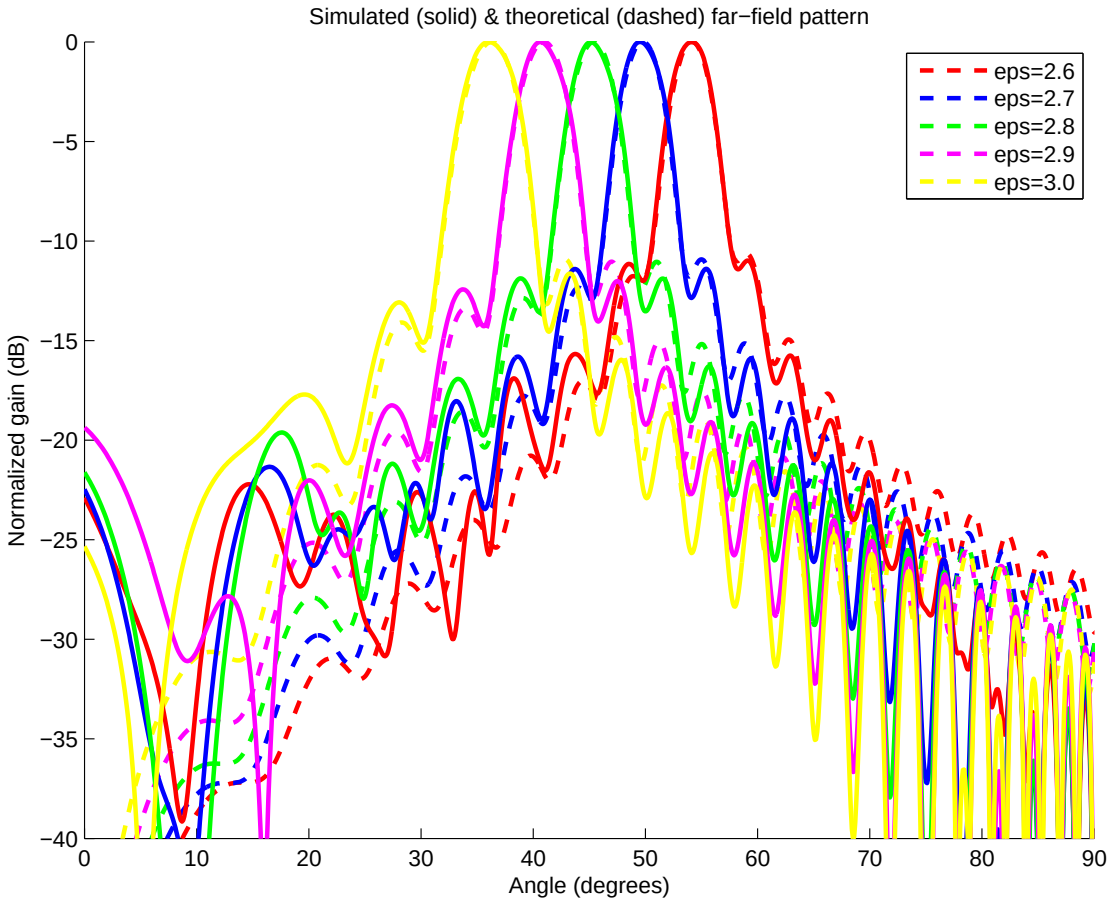

Figure 5.11: Normalized gain comparison between theoretical model and simulation results

5.5 Conclusion

The proposed NRD structures with asymmetric and symmetric feeding have been simulated for the parameters that have established in the previous chapters. The key concept to convey is that that double-degree frequency-dielectric reconfiguration has been demonstrated.

If one assumes the desired operational range to be the tuning states that correspond to the lower right half corner of the reconfiguration matrices corresponding to relatively high gain and "nice" beams then for both structures the following conclusions are valid:

1. a tunable angular range between approx. 50° and 20° is attainable.
2. an antenna gain of 15dB is realizable [4].
3. an 800MHz -3dB bandwidth is realistic.

Impedance matching The symmetric structure displays decent impedance matching over the full unlicensed 60G-band and can be considered broadband w.r.t. the asymmetric-

[4]Note that this is easily scalable by increasing/shortening the antenna length

caly fed antenna. The asymmetric structure becomes matched (approx. 1GHz assuming -10dB threshold) at very specific frequencies only that shift for different dielectric constants. This severely impairs the double-degree reconfiguration that is ambitioned in this research.

Beam quality The symmetric structure displays nice pure antenna beams for sufficiently high frequency/dielectric constant value combinations (the lower right corner in the reconfiguration matrices). The asymmetric feed however displays unexpected undesired mode excitation resulting in ugly radiation patterns.

6 Conclusion

6.1 Summary

The aim of this research has been to study a novel type of reconfigurable antenna based on a liquid crystal tunable dielectric. This has been achieved by proposing to equip a leaky-wave antenna based on non-radiative dielectric (NRD) waveguide with the mentioned liquid crystals. The unlicensed 60G frequency band has been selected as target of operation.

Initially a rectangular waveguide feed was considered. However, in a later stage this approach has been abandoned in favor of direct coaxial feeding.

Both approaches have been studied by means of performing full-wave simulations as well as the development of a prototype [1]. After performing an experiment with mentioned prototypes turned out to be too cumbersome the research came to rely on simulation data only, the result of which is presented in this thesis.

It has been proposed to replace the normally static NRD dielectric with the liquid crystals, while keeping them contained between the conducting plates and a foam container. A hypothetical voltage source applied to the conducting plates allows for tuning of the liquid crystals. A semi-rigid coaxial feed (penetrating the foam container) positioned at either the center or one end provides for the excitation of a leaky-wave. Both feed positions are investigated and are referred to as the so-called symmetric and asymmetric antenna structure. The former structure features a double symmetric radiation pattern whereas the latter has a single beam only. Finally, a particular type of liquid crystal called BL006 has been selected. This however has only been relevant to make realistic assumptions on the attainable effective permittivities.

The structures have been modelled using the numerical full-wave solver CST Microwave Studio and simulations have been performed using its so-called transient time-domain solver. Input to the solver have been structure dimensions as parameters. Frequency range and dielectric constants have acted as variables for which relevant data such as far-field antenna gain, input reflection, etc. have been computed.

In addition, special processing of the produced data has been post-processed using the Matrix-Pencil method, allowing waveforms to be decomposed in terms of decaying exponentials, thereby proving the existence of leaky waves.

[1] The rectangular waveguide prototype was developed at Fraunhofer FHR whereas the coaxial prototype has been developed at Delft University of Technology, Faculty of EEMCS

6.2 Findings

The key finding and contribution of this research is providing a proof-of-concept for antenna reconfiguration by changing either the operating frequency or the effective permittivity (through static voltage application).

For both structures it can be stated that (ignoring impedance mismatch) a 30° scanning range can be achieved with an associated gain of 15dB. However, this is only valid for a subset of all the possible tuning states. This is explained in more details in chapter 5. Furthermore, for the same tuning states a -3dB bandwidth of roughly 800MHz has been estimated to be realistic.

The symmetric structure appears to outperform the asymmetric structure for two reasons.

First, the asymmetric structure has a very poor (very frequency selective) impedance matching with its coaxial feed whereas the symmetric structure appears to be matched over the entire 60G-band. As a consequence, freedom in antenna reconfiguration (by switching operating frequency) is severely limited.

Second, the reflections from the wall impinge on the asymmetrically positioned coax feed. These collissions appear to excite undesired leaky modes in a rather unpredictable manner causing unallowable distortions in the radiation pattern. The symmetric structure does not suffer from this drawback.

6.3 Recommendations for further research

Recommendations for further research into this topic are both related to antenna design and (mechanical) prototyping and have been listed here in order of importance.

Containing liquid crystals It would be of extreme value to find a reliable way to keep the liquid crystals confined within the cavity. In the current approach the liquid seeps through the crevice between the foam and the metallic conducting plates preventing the experimentation with the designed protoype. At this point no experimental verification is possible of the proposed structure.

Verification of two-way tunability Tunability in one direction is done by the application of a static electric field. However, it remains to be seen that the reverse, reorientation of the crystals through surface grooves, can be achieved. The distances between the plates is relatively large (2mm). It needs to be verified whether this distance is small enough for achieving two-way tunability. This can obviously only be done when the above issue pertaining the containing of the LC is solved.

Prevention of undesired mode excitation It has been shown that undesired leaky-waves are sometimes excited. It could perphaps be realistic to aim for the excitation of a mode with lower cutoff frequency. For this a thorough analysis of the spectrum of supported modes is necessary. More specifically for the asymmetric structure, some additional

tweaking (lowering) of the amount of coaxial insertion into the liquid may result in less input reflection from the reflected wave and therefore less unwanted mode excitation.

Expansion or shifting of frequency range This research has focussed on the 60G unlicensed frequency range. These artifical bounds unnecessarily limit the full exploration of the proposed antenna's reconfiguration capacities. It would definitely be of interest to expand the study across the chosen borders. Moreover, one could consider shifting the frequency range altogether since LCs remain low loss for extremly high frequencies.

References

[1] C. Panagamuwa, A. Chauraya, and J. Vardaxoglou, "Frequency and beam reconfigurable antenna using photoconducting switches," *IEEE Transactions on Antennas and Propagation*, vol. 54, pp. 449–454, Feb 2006.

[2] C. Caloz, T. Itoh, and A. Rennings, "CRLH metamaterial leaky-wave and resonant antennas," *Antennas and Propagation Magazine, IEEE*, vol. 50, pp. 25–39, Oct 2008.

[3] N. Haider, D. Caratelli, and A. Yarovoy, "Recent developments in reconfigurable and multi-band antenna technology," *International Journal of Antennas and Propagation*, 2013.

[4] C. Christodoulou, Y. Tawk, S. Lane, and S. Erwin, "Reconfigurable antennas for wireless and space applications," *Proceedings of the IEEE*, vol. 100, no. 7, pp. 2250–2261, 2012.

[5] S. Sharma, M. Gupta, and C. Tripathi, "Reconfigurable antennae: A review," *International Journal of Electronics & Communication Technology"*, vol. 2, no. 3, pp. 131–135, 2011.

[6] J. Bernhard, *Reconfigurable Antennas*. Synthesis lectures on antennas #4, Morgan & Claypool, 2007.

[7] J. Kiriazi, H. Ghali, H. Ragaie, and H. Haddara, "Reconfigurable dual-band dipole antenna on silicon using series mems switches," in *Antennas and Propagation Society International Symposium, 2003. IEEE*, vol. 1, pp. 403–406 vol.1, June 2003.

[8] W. Weedon, W. Payne, and G. Rebeiz, "Mems-switched reconfigurable antennas," in *Antennas and Propagation Society International Symposium, 2001. IEEE*, vol. 3, pp. 654–657, July 2001.

[9] D. Sievenpiper, J. Schaffner, J. Lee, and S. Livingston, "A steerable leaky-wave antenna using a tunable impedance ground plane," *Antennas and Wireless Propagation Letters, IEEE*, vol. 1, no. 1, pp. 179–182, 2002.

[10] A. Gaebler, A. Moessinger, F. Goelden, R. Jakoby, *et al.*, "Liquid-crystal reconfigurable antenna concepts for space applications at microwave and millimeter waves," *International Journal of Antennas and Propagation*, 2009.

[11] L. Liu and R. Langley, "Electrically small antenna tuning techniques," in *Antennas Propagation Conference, 2009. LAPC 2009. Loughborough*, pp. 313–316, Nov 2009.

[12] L. Liu and R. Langley, "Liquid crystal tunable microstrip patch antenna," *Electronics Letters*, vol. 44, pp. 1179–1180, September 2008.

[13] N. Martin, P. Laurent, C. Person, P. Gelin, and F. Huret, "Patch antenna ad-

justable in frequency using liquid crystal," in *Microwave Conference, 2003 33rd European*, pp. 699–702, Oct 2003.

[14] A. Moessinger, R. Marin, S. Mueller, J. Freese, and R. Jakoby, "Electronically reconfigurable reflectarrays with nematic liquid crystals," *Electronics Letters*, vol. 42, pp. 899–900, August 2006.

[15] C. Damm, M. Maasch, R. Gonzalo, and R. Jakoby, "Tunable composite right/left-handed leaky wave antenna based on a rectangular waveguide using liquid crystals," in *Microwave Symposium Digest (MTT), 2010 IEEE MTT-S International*, pp. 13–16, May 2010.

[16] R. Daniels and R. Heath, "60 ghz wireless communications: emerging requirements and design recommendations," *Vehicular Technology Magazine, IEEE*, vol. 2, pp. 41–50, Sept 2007.

[17] A. Galli, F. Frezza, and P. Lampariello, "Leaky wave antennas," in *Encyclopedia of RF and Microwave Engineering*, pp. 2294–2303, John Wiley & Sons, Inc., 2005.

[18] D. R. Jackson and A. A. Oliner, "Leaky-wave antennas," in *Modern Antenna Handbook* (C. A. Balanis, ed.), pp. 325–367, John Wiley & Sons, Inc., 2007.

[19] A. Sanchez and A. Oliner, "A new leaky waveguide for millimeter waves using non-radiative dielectric (nrd) waveguide-part i: Accurate theory," *Microwave Theory and Techniques, IEEE Transactions on*, vol. 35, pp. 737–747, Aug 1987.

[20] P. Burghignoli, G. Lovat, and D. Jackson, "Analysis and optimization of leaky-wave radiation at broadside from a class of 1-d periodic structures," *IEEE Transactions on Antennas and Propagation*, vol. 54, pp. 2593–2604, Sept 2006.

[21] G. Lovat, P. Burghignoli, and D. Jackson, "Fundamental properties and optimization of broadside radiation from uniform leaky-wave antennas," *IEEE Transactions on Antennas and Propagation*, vol. 54, pp. 1442–1452, May 2006.

[22] D. Jackson, C. Caloz, and T. Itoh, "Leaky-wave antennas," *Proceedings of the IEEE*, vol. 100, pp. 2194–2206, July 2012.

[23] C. Caloz, "Metamaterial dispersion engineering concepts and applications," *Proceedings of the IEEE*, vol. 99, pp. 1711–1719, Oct 2011.

[24] S. Paulotto, P. Baccarelli, F. Frezza, and D. Jackson, "A novel technique for open-stopband suppression in 1-d periodic printed leaky-wave antennas," *IEEE Transactions on Antennas and Propagation*, vol. 57, pp. 1894–1906, July 2009.

[25] D. Deslandes and K. Wu, "Substrate integrated waveguide leaky-wave antenna: Concept and design considerations," *Asia Pacific Microwave Conference Proceedings*, 2005.

[26] M. Bozzi, A. Georgiadis, and K. Wu, "Review of substrate-integrated waveguide circuits and antennas," *Microwaves, Antennas Propagation, IET*, vol. 5, pp. 909–920, June 2011.

[27] J. Liu, D. Jackson, and Y. Long, "Substrate integrated waveguide (siw) leaky-wave antenna with transverse slots," *IEEE Transactions on Antennas and Propagation*, vol. 60, pp. 20–29, Jan 2012.

[28] A. Giere, Y. Zheng, H. Maune, M. Sazegar, F. Paul, X. Zhou, J. Binder, S. Muller, and R. Jakoby, "Tunable dielectrics for microwave applications," in *Applications of Ferroelectrics, 2008. ISAF 2008. 17th IEEE International Symposium on the*, vol. 2, pp. 1–2, Feb 2008.

[29] R. Marin, *Investigations on Liquid Crystal Reconfigurable Unit Cells for mm-Wave Reflectarrays*. PhD thesis, Technische Universität, Darmstadt, August 2008.

[30] Y. Utsumi and T. Kamei, "Dielectric permittivity measurements of liquid crystal in the microwave and millimeter wave ranges," *Molecular Crystals and Liquid Crystals*, vol. 409, no. 1, pp. 355–370, 2004.

[31] T. Sarkar and O. Pereira, "Using the matrix pencil method to estimate the parameters of a sum of complex exponentials," *Antennas and Propagation Magazine, IEEE*, vol. 37, pp. 48–55, Feb 1995.

Solver

A

In this research full-wave simulations have been performed with CST Microwave Studio 2011.

Settings The settings of each simulation are as default configuration unless listed below.

- Solver:
  - solver type: transient
  - accuracy: -30dB
- Meshing:
  - automatic mesh generation
  - mesh type: FPBA
  - refine at PEC by factor: 4
  - lines per wavelength: 15
  - lower mesh limit: 5
  - mesh ratio limit

Materials All materials used are either isotropic lossless or perfectly electrically conducting (PEC). No material has been modelled as lossy or anisotropic.

Matrix-Pencil method

B

The Matrix pencil method is an algorithm that is used to decompose any discrete series in terms of complex exponentials. In this research detection of a leaky-wave within a waveguide is achieved by applying this algorithm to the waveform as produced by the full-wave solver. The algorithm is introduced and described in [31].

The algorithm takes as input any (discrete) waveform $y(kT)$ (with sample number k and step size T) and decomposes it as follows

$$y(kT) = \sum_{i=1}^{M} R_i \cdot z_i^k \tag{B.1}$$

$$z_i = e^{(-\alpha_i + j\beta_i)T} \tag{B.2}$$

where M is the number of desired components one would like to extract. In addition it takes an additional parameter L, functioning as a sliding window. Throughout this work L = N/3 has been assumed as has been recommended by the author. The algorithm has been directly copied from and implemented in MATLAB as has been shown below.

The output of the algorithm are coefficients R_i and complex poles z_i with which a complex exponential series can be constructed.

B.1 Algorithm code

```
    subvec = @(vec,off,len) vec(1+off:off + len);
    y1 = zeros(N-L,L); y2 = zeros(N-L,L); % pre-allocate
    for j = 1 : N - L
        y1(j,:) = subvec(vec_in,j-1,L);
        y2(j,:) = subvec(vec_in,j,L);
    end
    y1_pi = pinv(y1);
    [~,D] = eig(y1_pi*y2);
    D_vec = diag(D);
    Z_vec = D_vec;

Z = zeros(N,L);
for i = 1 : N
    for j = 1 : L
        Z(i,j) = Z_vec(j)^(i - 1);
    end
end
```

```
R = Z\vec_in;

[R_sort, SortInd] = sort(R, 'descend');
Zi_sort = Z_vec(SortInd);

Ri_out = R_sort(1:M); % This contains the coefficients (output of
    algorithm)
Zi_out = Zi_sort(1:M); % This contains the complex poles (output of
    algorithm)
```

C

Modal patterns

The figures below give an impression of the modal patterns of three modes as computed by CST Microwave Studio. The QTEM-mode is undesired because it is not a fast wave and therefore does not radiate. The hybrid mode shown in Figures C.1c and C.2c has been selected as the desired mode because its appears to be excited well by the coaxial probe.

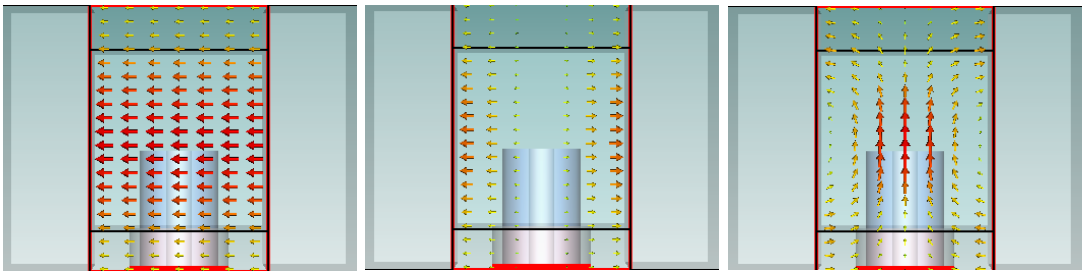

(a) QTEM (b) Hybrid I (hor. E-field) (c) Hybrid II (vert. E-field)

Figure C.1: Modal patterns: E-field ($\phi = 0$)

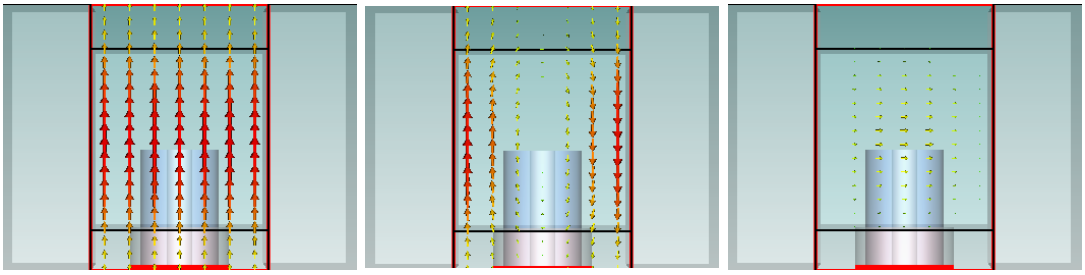

(a) QTEM (b) Hybrid I (vert. H-field) (c) Hybrid II (hor. H-field)

Figure C.2: Modal patterns: H-field ($\phi = 0$)

Datasheets

D

D.1 Semi-rigid coax

In fig. D.1 an extract from a datasheet containing standardized semi-rigid coaxial cables from the supplied JYEBAO is shown. The relevant values are highlighted. The cross-sectional dimensios are referred to in chapter 3. For the full-wave simulations a dielectric constant of $\epsilon_r = 2.1$ has been assumed for PTFE material. Also it can be observed that the operated frequency range is far away from the cut-off point of 1st-order higher mode propagation.

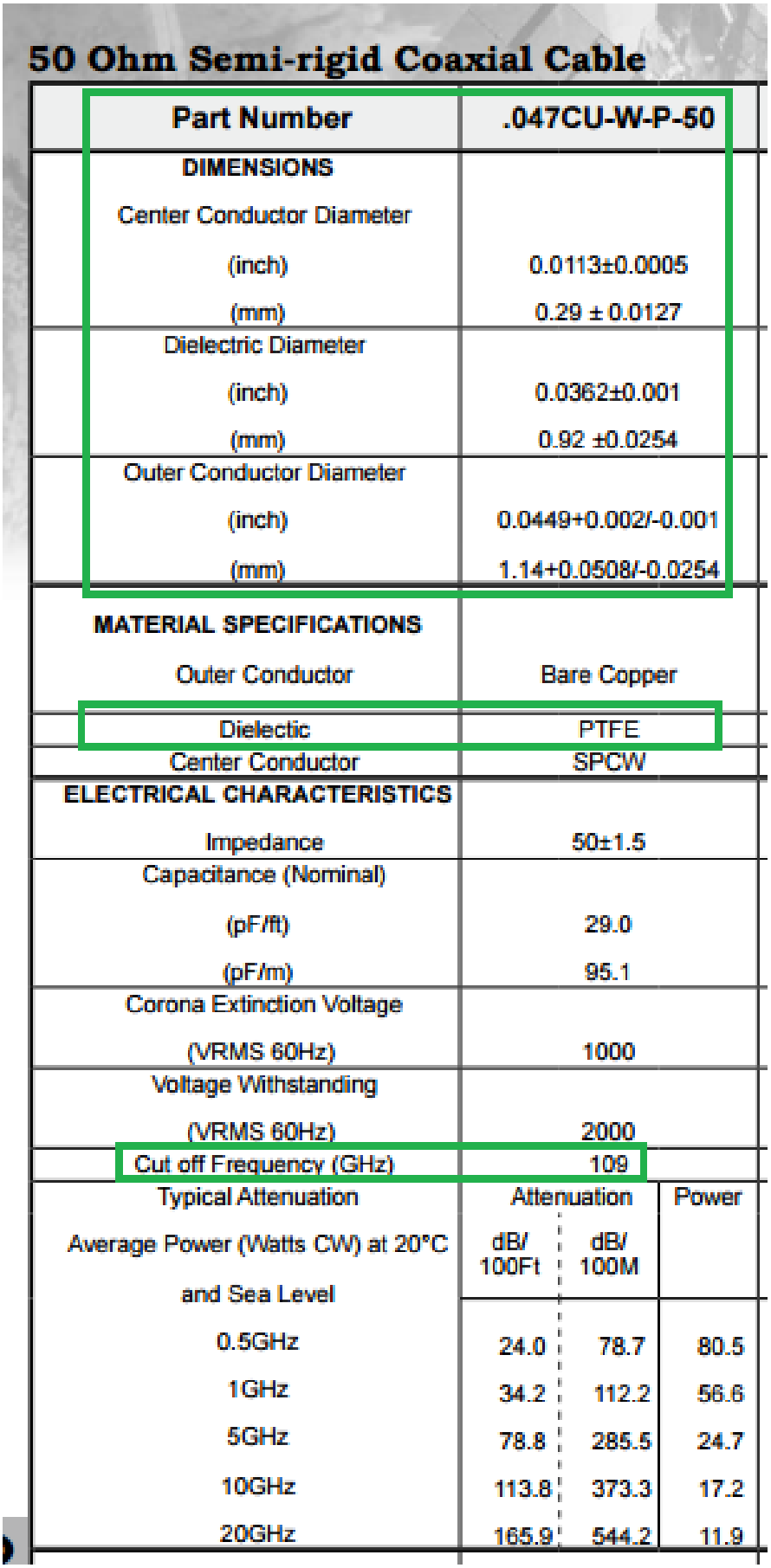

50 Ohm Semi-rigid Coaxial Cable

Part Number	.047CU-W-P-50		
DIMENSIONS			
Center Conductor Diameter			
(inch)	0.0113±0.0005		
(mm)	0.29 ± 0.0127		
Dielectric Diameter			
(inch)	0.0362±0.001		
(mm)	0.92 ±0.0254		
Outer Conductor Diameter			
(inch)	0.0449+0.002/-0.001		
(mm)	1.14+0.0508/-0.0254		
MATERIAL SPECIFICATIONS			
Outer Conductor	Bare Copper		
Dielectic	PTFE		
Center Conductor	SPCW		
ELECTRICAL CHARACTERISTICS			
Impedance	50±1.5		
Capacitance (Nominal)			
(pF/ft)	29.0		
(pF/m)	95.1		
Corona Extinction Voltage			
(VRMS 60Hz)	1000		
Voltage Withstanding			
(VRMS 60Hz)	2000		
Cut off Frequency (GHz)	109		
Typical Attenuation	Attenuation		Power
Average Power (Watts CW) at 20°C and Sea Level	dB/ 100Ft	dB/ 100M	
0.5GHz	24.0	78.7	80.5
1GHz	34.2	112.2	56.6
5GHz	78.8	285.5	24.7
10GHz	113.8	373.3	17.2
20GHz	165.9	544.2	11.9

Figure D.1: Extract from standardized semi-rigid coax datsheet